PART I: MICROWAVE STUDIES OF NONIONIZING SHOCK WAVES

by
S. TAKEDA
L. GOLDSTEIN
M. ROUX

PART II: A PROPOSED MICROWAVE REFLECTION METHOD FOR THE STUDY OF HIGH ENERGY SHOCK WAVE PRODUCED HIGH DENSITY PLASMAS

by
S. TAKEDA
M. ROUX

Technical Report No. 2
Contract DA-36-039-SC-78313
File No. 18716-PM-59-91-91 (4967)

1 July 1962

Sponsored by
U. S. ARMY
SIGNAL CORPS ENGINEERING LABORATORY
Fort Monmouth, New Jersey

ELECTRICAL ENGINEERING RESEARCH LABORATORY
ENGINEERING EXPERIMENT STATION
UNIVERSITY OF ILLINOIS
URBANA, ILLINOIS

PART I: MICROWAVE STUDIES OF NONIONIZING SHOCK WAVES

by

S. TAKEDA

L. GOLDSTEIN

M. ROUX

PART II: A PROPOSED MICROWAVE REFLECTION METHOD FOR THE STUDY OF HIGH ENERGY SHOCK WAVE PRODUCED HIGH DENSITY PLASMAS

by

S. TAKEDA

M. ROUX

Technical Report No. 2

Contract DA-36-039-SC-78313

File No. 18716-PM-59-91-91(4967)

1 July 1962

Sponsored by

U. S. ARMY

SIGNAL CORPS ENGINEERING LABORATORY

Fort Monmouth, New Jersey

ELECTRICAL ENGINEERING RESEARCH LABORATORY

ENGINEERING EXPERIMENT STATION

UNIVERSITY OF ILLINOIS

URBANA, ILLINOIS

ABSTRACT

The interaction of microwaves with gaseous plasmas is used to study weak shock waves in low pressure gases. An improved technique for microwave measurement of plasma parameters is used which is applicable to plasmas, varying rapidly with time. By this method the electron density and the collision frequency in a plasma are deduced from the simultaneous recording of two microwave detector signals. The validity of this method was tested in a decaying plasma created by a pulsed DC discharge in the usual way.

In this method the gas is weakly pre-ionized and shock waves with a Mach number too low to ionize the gas are then propagated. Using a tube 5mm in diameter and condenser discharges for the production of shock waves up to 200 joules with Mach number up to 5 in a pressure of 4 to 13 mmHg in Neon and Argon, it is found that the measured electron density increased across the shock discontinuities in the ratio of the gas density ratio. The electron temperature, deduced from the measured electron-ion collision frequency is, as expected, lower than the gas temperature estimated from the Mach number

In addition to the electromagnetic behavior the optical properties of the plasma are put to use in these studies These properties provide us with an independent source of information which is directly correlated with the microwave measurements.

Finally, a method for measuring the higher electron densities in plasmas is proposed.

CONTENTS

ILLUSTRATIONS

ILLUSTRATIONS (Continued)

PART I

MICROWAVE STUDIES OF NONIONIZING SHOCK WAVES

by

S. Takeda

L. Goldstein

M. Roux

1. INTRODUCTION

It has been observed in the early phases of our work on TR spike investigation[1] that when rapid discharges occurred in TR cavities the transmitted but attenuated RF signal appeared to be modulated during a more or less extended time interval following the magnetron pulse. This phenomenon was then attributed by us to an oscillatory motion of the ionized and also non-ionized gas, but the phenomenon could not be investigated then in any detail because of lack of time.

Before starting with RF discharges, we investigated these and similar phenomena in a pulsed DC discharge. Experiments were begun with discharge tubes of simple and usual geometries.

It is now known that shock waves are detected in heavy condenser discharges, particularly in relatively low pressure gases. These shock wave phenomena will be the subject of the initial part of these investigations.

The main broad historical steps appear to be the following. The first observation of a bright luminescence in a tube connected perpendicularly to a main tube in which RF discharges had been ignited without electrodes was reported by R. L. Rayleigh.[2] R. F. Fowler[3] found that a luminous wave propagated at a velocity higher than sound in the side branch of a T-shaped gas discharge tube, after a strong discharge had been ignited with internal electrodes in the main tube. M. Cloupeau[4] also showed clear photographs of light intensity variations in the afterglow of a condenser discharge excited in Xe at 10 mmHg. This was attributed to longitudinal and lateral shock waves. More recently, measurements have been performed on shock waves and many papers have reported results obtained by studying shock waves using optical and spectrospical methods. Measurements using microwave techniques have also been reported.[5,6]

Schultz[6] noticed that it would be possible to determine by microwave techniques both electron density and collision frequency in a plasma produced by an ionizing shock wave. However, since a microwave signal is generally highly attenuated when it propagates through a

plasma produced in a low pressure gas the propagation method using such a microwave signal is restricted in its application. This attenuation is caused by the fact that the plasma frequency associated with the electron density reaches a critical value corresponding to the microwave frequency. The impedance of a small volume of plasma, however, can be measured at higher densities provided a condition presented in 7 is satisfied. If the method reported here satisfies this condition, the range of measurements can be extended to electron densities higher than the critical value.

Usually microwave techniques for the investigation of plasma impedance are based on the shift of the minimum amplitude position of a standing-wave detector and on the change of the standing-wave ratio, but when the plasma is produced by a non-recurrent (one-shot) discharge, these standard techniques become inadequate. Since the initial conditions of such weak transient discharges are not always reproducible as exactly as in the case of a weak recurrent discharge, a modified method of microwave measurement is here developed using time resolved photographs of the microwave standing wave amplitude which yield both the electron density and collision frequency. By using these techniques shock waves produced by electrical discharges have been investigated.

The method requires a minimum detectable electron density, and when strong shocks are studied, this is provided by the ionizing shock waves themselves. However, in order to study weak, that is non-ionizing, shocks a plasma with the appropriate electron density has to be provided by auxiliary pre-ionization, as used by der Agobian[5].

2. SOME PRELIMINARY EXPERIMENT OF SHOCK DETECTION

We planned at first to determine the propagation velocity of the shock wave by using phototubes to measure the discontinuities in the light emitted by the tube. The simple arrangement of the apparatus is shown in Figure 1. A strong pulsed discharge was ignited between electrodes 1 and 2 in a tube which had a construction similar to that used by V. Josephson.[8] The electrode 4 and outside strip electrode 3 were used to ignite an auxiliary pulsed discharge. There are two holes in the box housing the phototube and each can be opened or closed independently. The output current from the phototube located 10 cm distance from electrode 2 is shown in Figure 2. Here pre-ionization was not used. The discharge was produced in Argon at the pressure of 15 mmHg. The first peak of increased light intensity in Figure 2 came from the main discharge, and the second smoother peak was due to the light emitted by recombination of electrons and ions which diffused from the region of the main discharge. The explanation of the latter effect was confirmed by the quenching of this afterglow when a heating microwave pulse was propagated through the region of interest at the appropriate time. However, the first peak of light intensity was later shown to be due to some component of current flowing from electrode 1 to electrode 4, since it disappeared when electrode 4 was not grounded.

If the gas has not been pre-ionized, the weak shock produced by the discharge traveling down the tube will not carry energy sufficient to ionize the neutral, unheated gas As a result of this failure of the forward traveling shock wave to ionize the neutral gas, its presence will not be detected by our light-measuring apparatus. However, the shock wave will be reflected at the end of the tube and travel back toward the discharge. The backward-traveling shock wave will be even weaker than the forward-traveling wave and will not produce visible light in the neutral, unheated gas either. However, an envelope of hot gas has been moving down the tube from the discharge

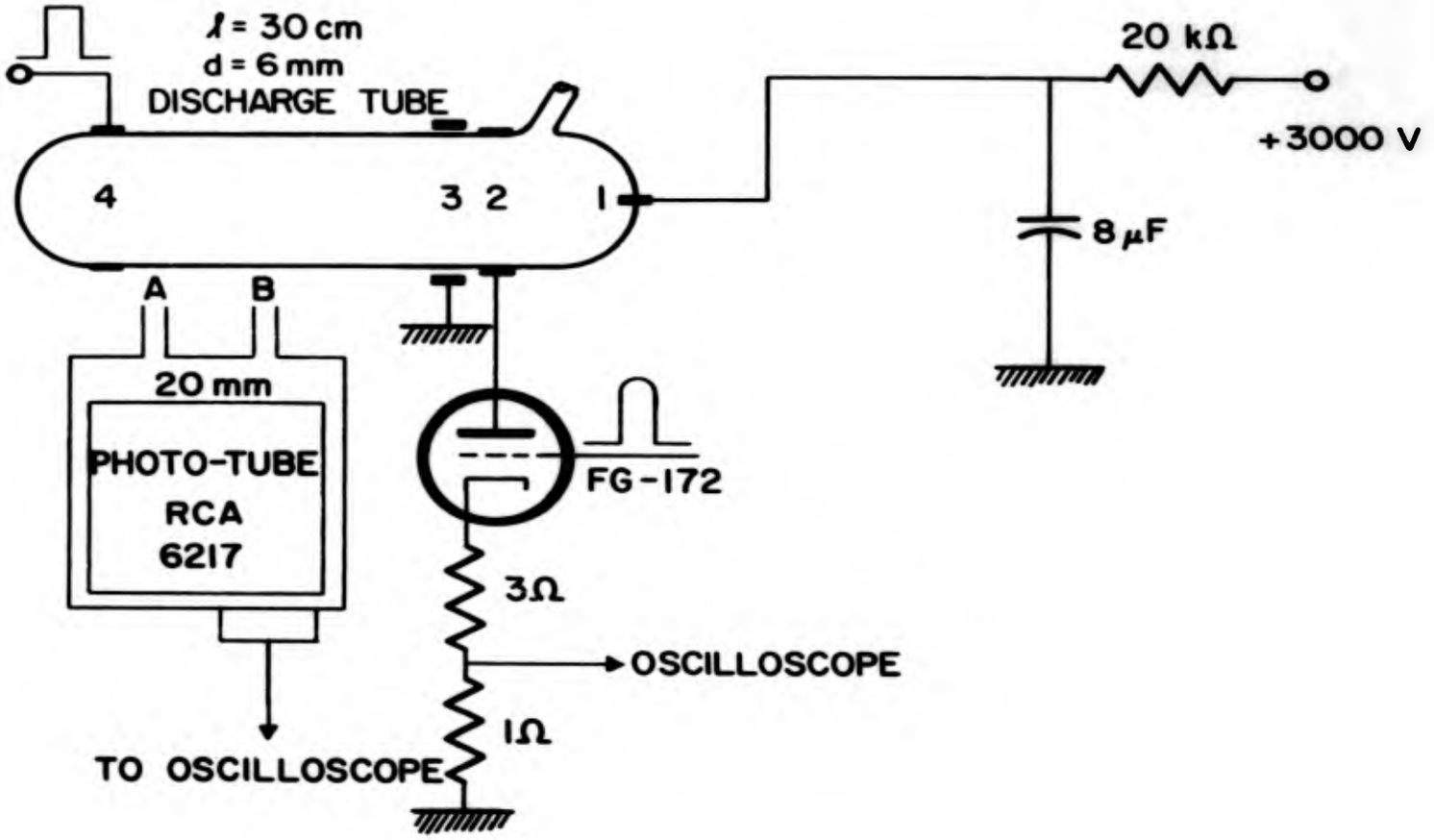

Figure 1. Total arrangement of the experimental system

in the wake of the shock wave. When the backward-traveling shock wave enters this region its low energy will still not be sufficient to cause ionization, but it will compress the gas and increase the recombination causing a corresponding increase in light intensity. This accounts for the discontinuity which occurs at about 1000 μsec in Figure 2. This discontinuity has been circled and drawn out of scale for emphasis. The discontinuity consists of two bumps, the first being due to light detected at the light detector position A, and the second to light detected 40 μsec later at B (See Figure 1). Light is detected at A before B, indicating that it is due to a backward-traveling wave. If the detector is placed more than 10 cm from the discharge no light can be seen at all. This is because the hot gas is traveling much slower than the shock wave. If the photocell is any further from the discharge the backward-traveling shock wave will have passed the observation point before the hot gas arrives and no light will be observed. The decrease in light intensity in Figure 2 after the shock wave has passed is due to a quenching of the afterglow by the heating effects of the shock wave.

When the shock was propagated in a pre-ionized gaseous medium the result was as that shown in Figure 3. The discontinuity found at 200 μsec in Figure 3 was attributed to the compression caused by the forward-traveling shock wave and was larger than that caused by the reflected wave in Figure 2. The pre-ionization was produced by an auxiliary discharge. In this case, the two peaks of the discontinuities had equal heights probably because the remaining electrons at that time were distributed uniformly along the axis of the tube. In this experiment, the forward propagation velocity was about 0.1 cm/μsec (which would correspond to a Mach number of 3). The corresponding value of the gas temperature was about 1000°K.[9] At this temperature the gas atoms cannot be ionized effectively, but some of them might be excited by the electrons produced in the auxiliary discharge.

The thyratron tube previously used cannot handle peak currents higher than several hundred amperes. To operate with higher current,

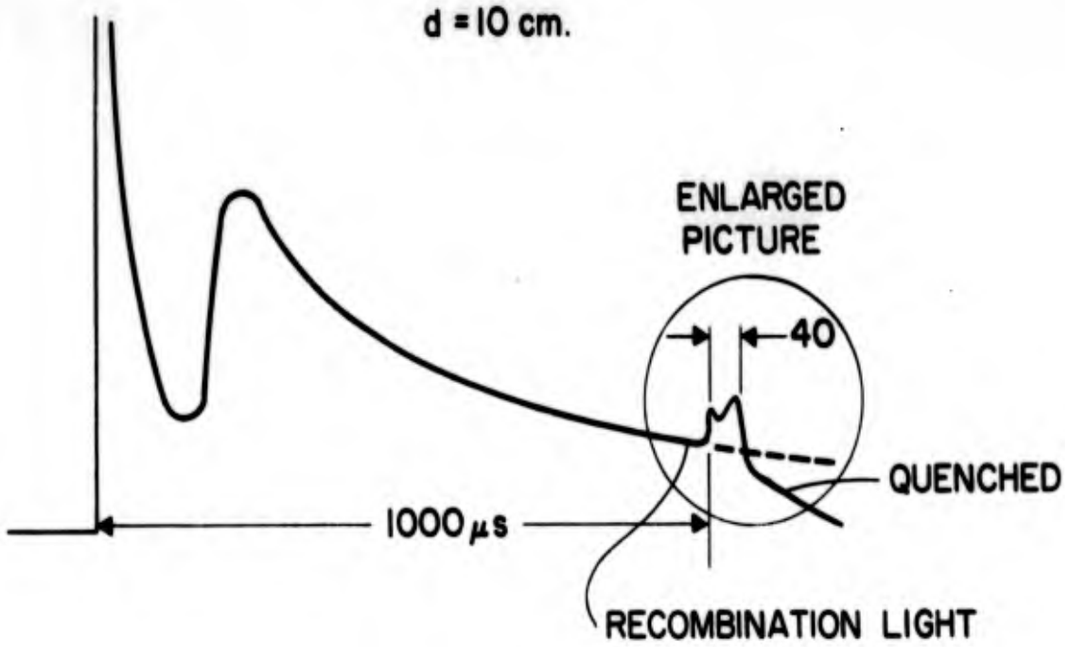

Figure 2. Light intensity without pre-ionization

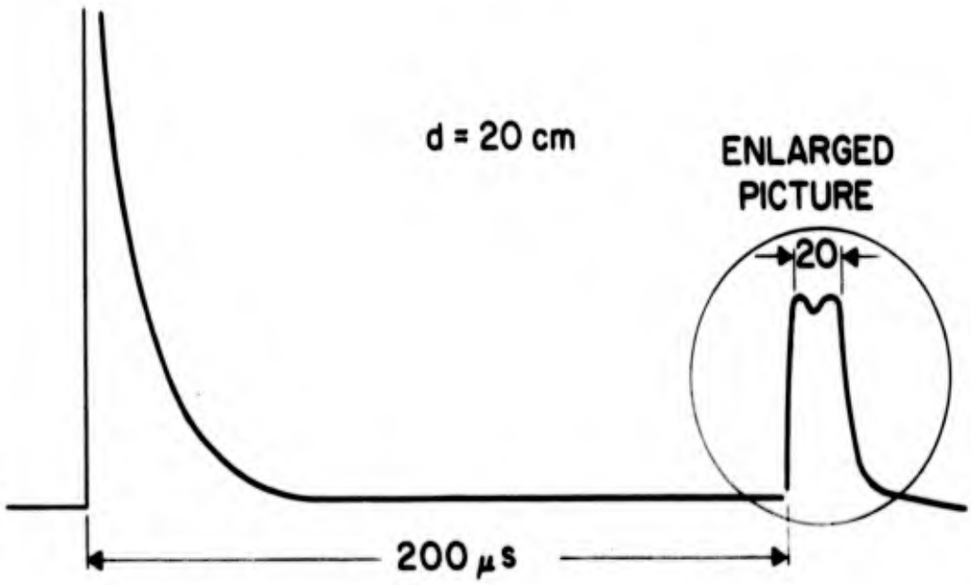

Figure 3. Light intensity with pre-ionization

a gap switch with a triggering electrode of the type reported by Cullington[10] was used. This gap switch is connected directly to the condenser terminal. The ringing frequency of the discharge circuit was 130kc and the inductance was 27 μH. The maximum voltage, energy, and mean current during the first half cycle was 7kv, 200 joules, and 2×10^4 A, respectively.

Since we are interested in shock waves which might be produced in TR tubes, we pulsed our phototube with a strong microwave discharge produced by a magnetron. Trials were made with and without pre-ionization, but due to the low power output (10kw) of the magnetron then available, no discontinuities attributable to shock waves were detected in the light. However, several peaks of light were observed propagating along the discharge tube during the afterglow. These were probably due to moving striations where small DC currents were flowing. The effect was eliminated by shunting the electrode with a 1 k Ω resistor. Such disturbances in the afterglow should be carefully avoided when a pulse discharge is used.

3. EXPERIMENTAL APPARATUS FOR SHOCK WAVE STUDIES

The apparatus consists of a shock tube and a microwave circuit as shown in Figure 4. The shock tube, which is 40 cm in length and 0.5 cm in diameter, is placed across two waveguides in which an x-band low level microwave signal is propagated. These waveguides may be placed at any desirable distance from one another and are connected through a directional coupler to the same microwave source. In order to increase the resolution one of these waveguides is tapered to a flat section. This waveguide is terminated with a movable short and has two probe detectors, one on each side of the shock tube. A fraction of the microwave energy is taken from the first waveguide through a directional coupler and propagates in the second waveguide where it is detected by the probe detector 3.

The shock waves are produced in the tube which is filled with a gas at the desired pressure by discharging an 8 μF condenser charged to 7kv between electrodes A and B. In order to reduce the ignition delay time the condenser discharge path is very weakly ionized by a small DC current passing between the electrodes A and B through a high resistance shunting the gap switch. In order to provide the plasma in which the shock wave will propagate, a pulsed DC discharge pre-ionizes the gas between electrodes B and C. As the shock wave travels down the tube it will disturb the decaying plasma, causing perturbations in the microwave transmission in the two waveguides. The standing wave produced in the first waveguide by the movable short is detected by probes 1 and 2 and displayed on an oscilloscope. This standing-wave is modulated by the plasma so that the perturbation of the plasma by the shock wave causes a clearly visible disturbance in the standing wave. From the time varying amplitude of these signals, the instantaneous impedance of the plasma can be determined, which in turn yields the plasma parameters n and ν in the absence as well as in the presence of the shock wave.

The signals from detectors 3 and 1 or 2 yield the time interval for the shock wave to propagate from the first to the second waveguide

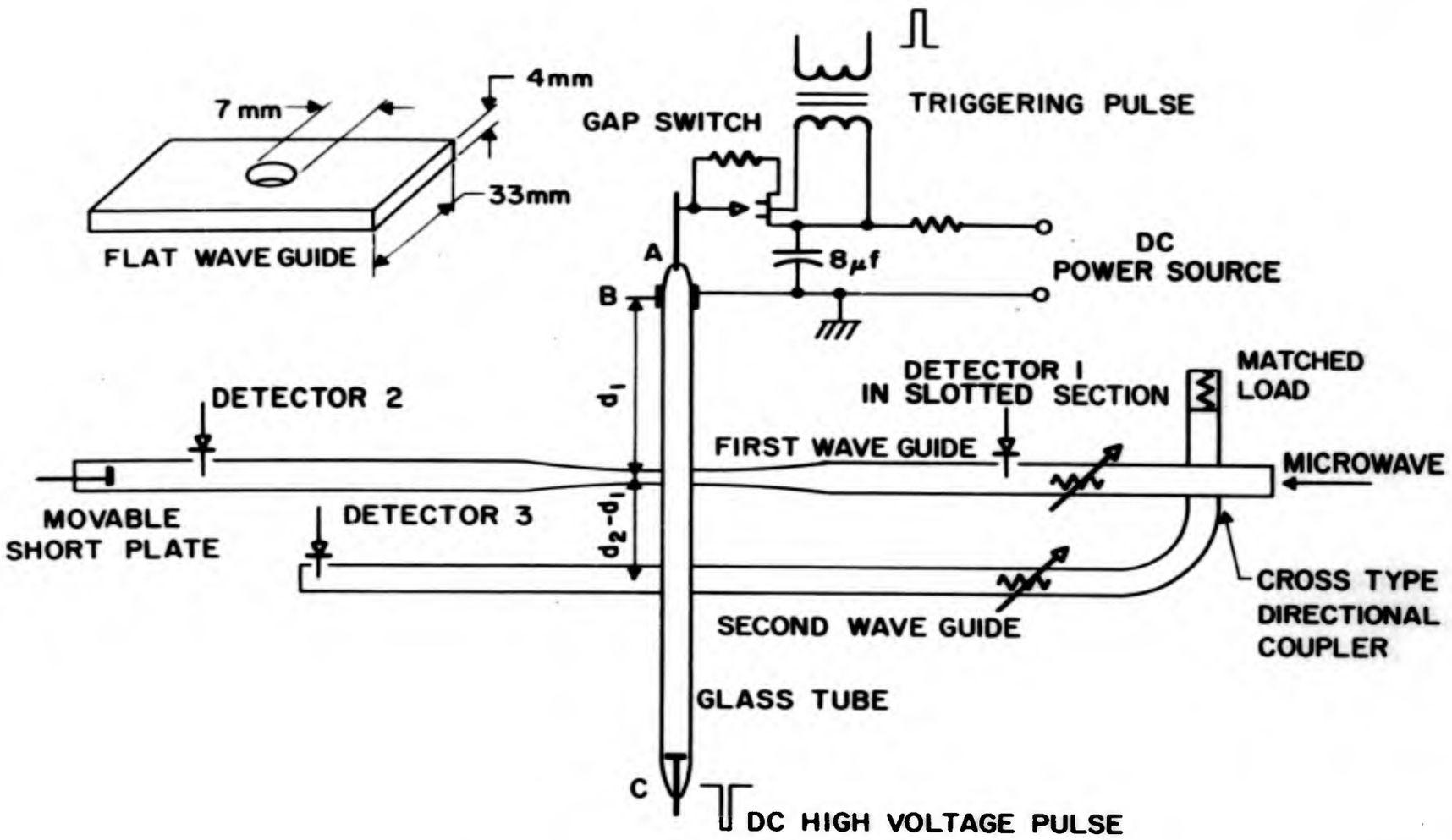

Figure 4. Diagram of the experimental apparatus

and hence its local velocity. Since the discharge is non-recurrent, the traces displayed on the oscilloscope are recorded photographically for analysis. Concurrently with the microwave observation, a photomultiplier is used for the detection of any discontinuity in the visible light intensity in the plasma afterglow.

A vacuum system was used to evacuate the tube down to pressures of 10^{-7} mm Hg. However an appreciable amount of impurities of metal vapor were produced at the electrodes during each condenser discharge. The presence of these impurities in the plasma was indicated by a change in color or by a shortened decay time However, when a recurrent DC discharge was set up in the tube, it was learned that the natural color of the gas soon returns, indicating that the metallic gases are deposited back on the electrodes or on the glass. Since it would be extremely inconvenient to replace the gas after each discharge the same gas was used, allowing for a sufficiently long time interval between discharges. The situation was improved by the use of activated charcoal maintained at low temperature in a side tube close to the electrodes A and B.

4. PRINCIPLES OF THE MEASUREMENTS

The method is capable of yielding the velocity of shock waves in plasmas and the variation of the background plasma parameters n and ν as a result of shock-wave propagation. The velocity of the propagating shock wave decreases as it proceeds along the tube. Hence one can speak about an average velocity over a length of propagation path and of a local or instantaneous velocity if the path is short with respect to the total path. When the distance d covered by the shock wave in time t takes the form $d = t^{\beta}$, the local velocity $v_t = \beta (d/t) = \beta x$ mean velocity $= \beta \bar{v}$. If a wave is found at d_1 at time t_1 and at d_2 at time t_2, β is determined from

$$\beta = \frac{\log d_2/d_1}{\log t_2/t_1} \qquad (1)$$

and $\bar{v}$ is equal to $\beta d^{\beta-1/\beta}$.

The initial conditions of the discharge cannot be reproduced exactly each time, hence the usual microwave techniques applicable to study the phenomena occurring regularly at high repetition rate are here inapplicable. In particular, the standard techniques to find the plasma impedance from the shift of the minimum position and the ratio of a standing wave produced in the waveguide by a recurrent plasma cannot be used here, and a modified method has been used. This method, contrary to other microwave propagation methods, is not strictly limited to measuring electron densities up to that value which corresponds to the critical plasma frequency, provided that the electron density along the tube axis is uniform. Although this is not strictly the case in these experiments in view of the small height of the plasma involved in the flat waveguide (4 mm), this assumption appears to be approximately justified.

At this point, attention should be drawn to the following. The amplitude of the signal in the first waveguide without plasma, at the minimum of the standing wave, is 0.005 of the amplitude at the maximum

of the standing wave. The existence of a detectable signal at the standing wave minimum is due to various losses in the microwave circuit. A large fraction of this loss is due to the energy leaking from the waveguide through the hole, accommodating the glass tube. In the presence of the plasma the microwave energy loss, which obviously includes the energy radiated through the hole, increases and is a function of the plasma parameters n and ν. In view of the lack of precise knowledge of this enhanced radiated energy loss, which occurs for large values of the electron density, the method at the present time is restricted in its application to values of the electron density smaller than this value. This fact also limits the range in which the electron collision frequency can be determined.

At one end of the waveguide circuit a cw, low power, X-band kylstron produces the microwaves at the desired frequency. This wave is reflected at the other end by a movable short and builds up as a standing wave as shown in Figure 5. The two microwave probe detectors are located on the waveguide, detector 1 on the klystron side, detector 2 on the short side of the tube. In the absence of plasma, detector 1 is at a minimum amplitude position , whereas detector 2 is in the vicinity of a maximum amplitude position. The equivalent circuit of the waveguide and plasma post, the standing wave pattern in the waveguide, and the respective positions of the probe detectors are shown in Figure 5.

The position of the short is adjusted in the absence of plasma so as to have a maximum of the standing wave at the tube axis. If the tube material had no effect on the standing wave pattern, the distance between the tube axis and the movable short would be an odd multiple of a quarter wavelength. However, inserting the glass tube in the waveguide is equivalent to inserting a capacitor. In order to have a voltage maximum (infinite impedance) at the center of the tube, the short circuit must be adjusted to a position where it will produce at the tube an inductive reactance equal in magnitude to the capacitive reactance due to the glass tube.

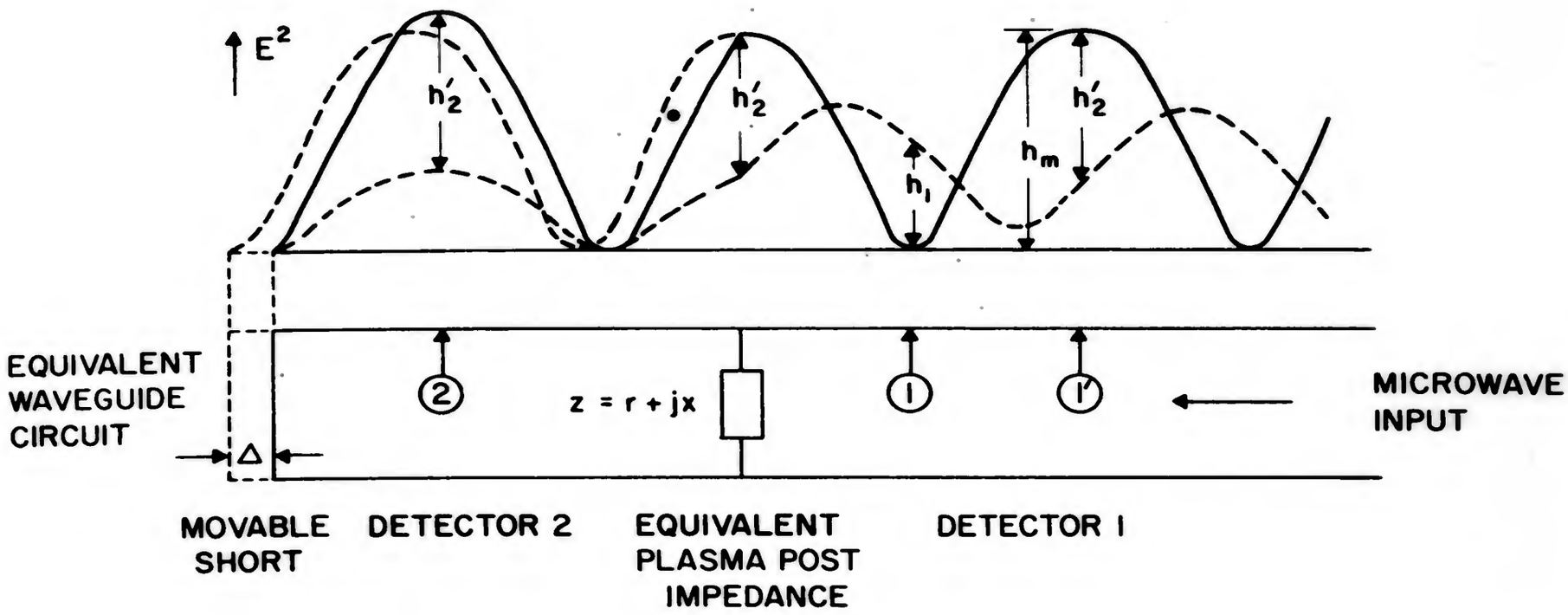

Figure 5. Equivalent wave guide circuit and microwave standing wave patterns. Solid line: without plasma but with glass, dashed line: with plasma and glass, dotted line: ideal case, without plasma and glass.

The normalized equivalent impedance of the plasma can be found from the change in the amplitude of the power due to the presence of the plasma detected by the two probes. We can then calculate the electron density n and the collision frequency ν from the normalized plasma impedance.

$$h_1 = 1/4 \left| 1 - \frac{Z - 1}{Z + 1} \right|^2$$

$$h_2 = 1 - 1/4 \left| 1 + \frac{Z - 1}{Z + 1} \right|^2 \qquad (2)$$

where the h's are the absolute differences between the powers detected by probes 1 and 2 with and without plasma normalized to the maximum amplitude of the microwave cut-off pulse h_m to have a maximum value of unity for z = 0. For convenience h_1 and h_2 were displayed simultaneously on the oscilloscope. The terms Z and (Z-1)/(Z+1) are respectively, the normalized impedance of the plasma and its reflection coefficient. Using Z = r + jx, r and x are solved from Equation (2),

$$x = \left[\frac{1}{h_1} - \left(\frac{h_1 + h_2}{2 h_1} \right)^2 \right]^{1/2}$$

$$r = \frac{h_2 - h_1}{2 h_1} \qquad (3)$$

The two components of the impedance are thus calculated from observed h_1 and h_2. The relation of $h_2 - h_1$ versus h_1 is plotted in Figure 6. The equivalent normalized impedance of a plasma post is given by a formula indicated by Markuvitz.[11] The complex dielectric constant in this formula is related to the electron density n and the collision frequency ν by

$$\xi = 1 - \frac{ne^2}{m \epsilon_o \omega} \quad \frac{1}{\omega + j \nu} \qquad (4)$$

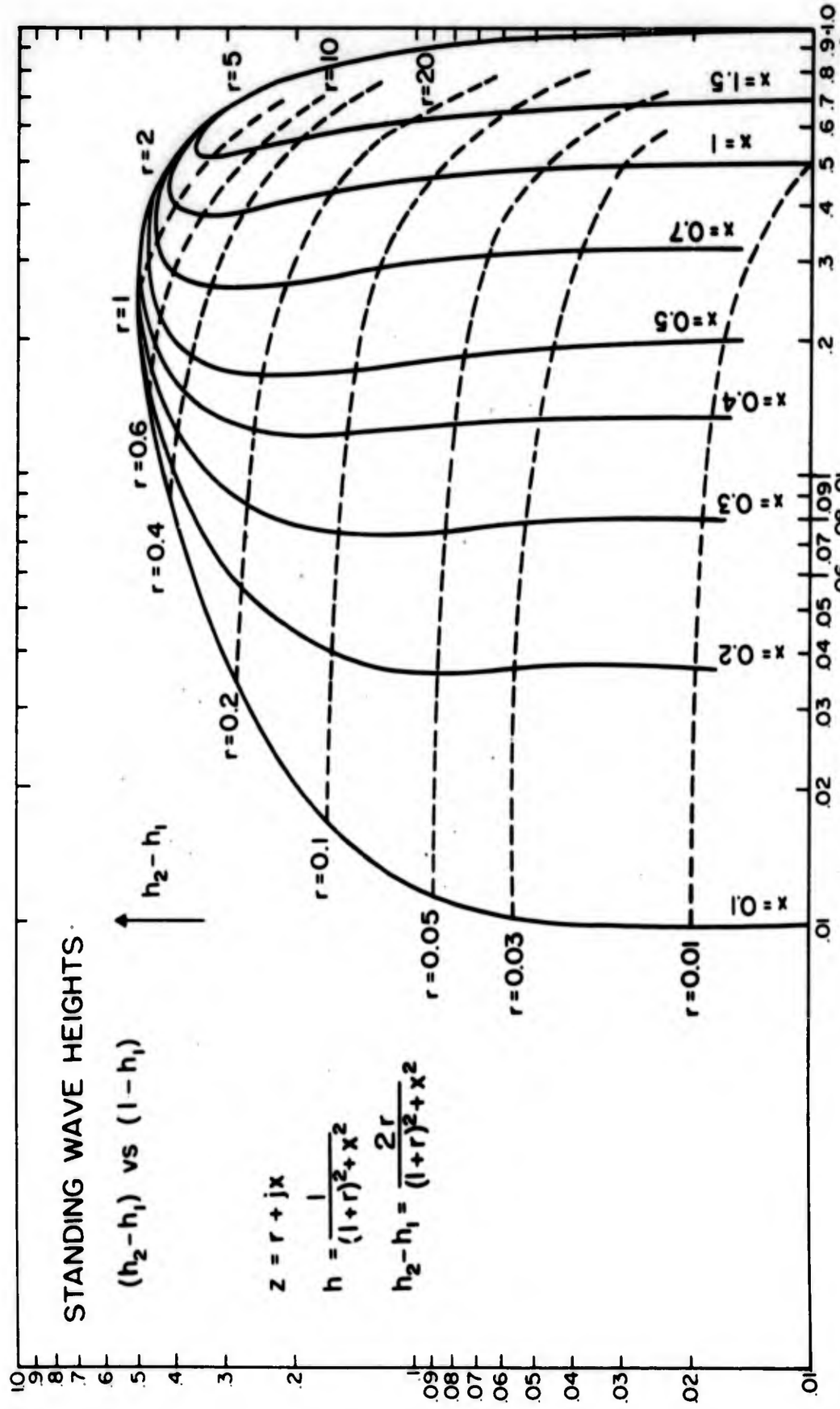

Figure 6. Chart representing r and x as functions of h_2-h_1 and h_1

When Equation (4) is put into the formula for the plasma impedance, the real and imaginary parts of Z can be separated, and finally n and ν are deduced, as

$$n = \frac{A}{x-B}$$

$$\nu/\omega = \frac{r}{x - B} \quad \text{or} \quad \nu/n = \frac{\omega r}{A} \tag{5}$$

where

$$A = \frac{m\epsilon_o \omega^2}{e^2} \left(\frac{a}{2\lambda_g}\right) \left\{0.50 + 2\left(\frac{\lambda}{\pi d}\right)^2\right\}$$

$$B = \frac{a}{2\lambda_g} (S_o + 0.25)^*$$

The constants A and B depend on the diameter of the plasma post d, the waveguide width a, and the free space wavelength λ and waveguide wavelength λ_g.

When x is very large compared to B,

$$n = \frac{A}{x_1} \qquad \nu/\omega = r/x \qquad (5')$$

Thus Equations (3) and (5) relate n and ν to the observed h_1 and h_2.

In this method, Equation (5) does not imply the condition $\nu \ll \omega$. However, there are some restrictions in the plasma impedance formula. They are:

---

*S_o is defined in Reference (11)

$$\sqrt{|\epsilon|} < 4$$

$$d/\lambda < 0.15 \qquad (6)$$

$$2a > \lambda > 2/3\, a$$

The relation n versus h_1, for X-band frequency and the conditions of our equipment, is shown in Figure 7 for different parameters of ν/n. Electron densities higher than the critical value can be measured, provided the electron distribution along the axis of the tube is uniform, because then the electric field is almost perpendicular to the gradient of the electron density and the AC space charge does not have a disturbing effect on the probing microwave field.[2] However, the restriction on ϵ, limits the maximum electron density to 2×10^{13} cm^{-3}.

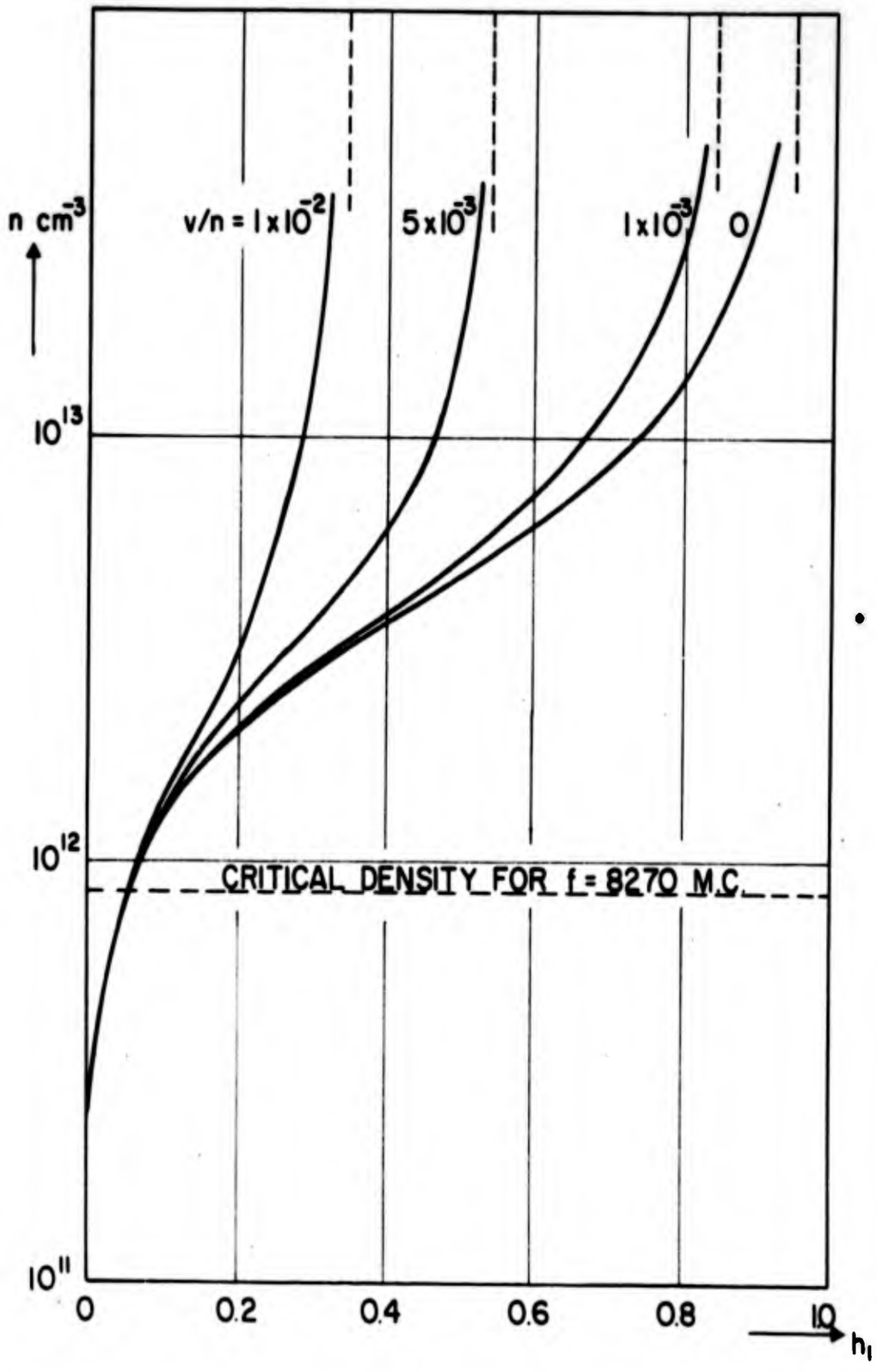

Figure 7. Electron density n versus normalized microwave signal amplitude h_1 of detector 1, for different values of the parameter v/n, where a = 33mm, d = 5mm are used

5. EXPERIMENTS ON A TYPICAL AFTERGLOW DISCHARGE

In order to confirm the applicability and the validity of this impedance measurement it was applied to a typical recurrent decaying plasma. Since the two detector signals are photographically recorded, the technique is especially adapted to plasmas produced by non-recurrent discharges.

The following procedure is used to find the correct position of the short. For some arbitrary position of the short in the absence of plasma, the probe of detector 1 is shifted a quarter wavelength from its minimum amplitude position to point 1 , a maximum. Now both probes 1 and 2 are at maximums. By adjusting the gain of the corresponding amplifiers the amplitudes of the probe signals on the oscilloscope are made equal. Then a discharge is produced in the tube by a repeated DC pulse of short duration and the effect of the plasma decay on the standing-wave pattern is observed.

It should be noted that for the arbitrary time of observation during the plasma decay shown in Figure 5 the standing wave pattern at the right side of the tube is shifted and attenuated with respect to its shape without plasma, whereas the one at the left side of the tube only decreases in amplitude but suffers no shifting. Therefore, during the plasma decay the amplitude change h_2' of probe signal 2 is always proportional to the amplitude change h_2' on the tube axis. However, the amplitude change of probe signal 1 is equal to h_2 only if the standing wave pattern at the right side of the tube has, without plasma, a maximum on the tube axis. This criteria is satisfied by a trial and error adjustment of the movable short, probe 1 being kept at a plasma-absent maximum, point 1 . The signals h_2 and h_1 will now coincide at all times after the first few microseconds when the high density plasma is disturbing the electric field in the waveguide. The accuracy of this method leads to a maximum mismatching in the probe position smaller than 5 mils or 1 electrical degree .

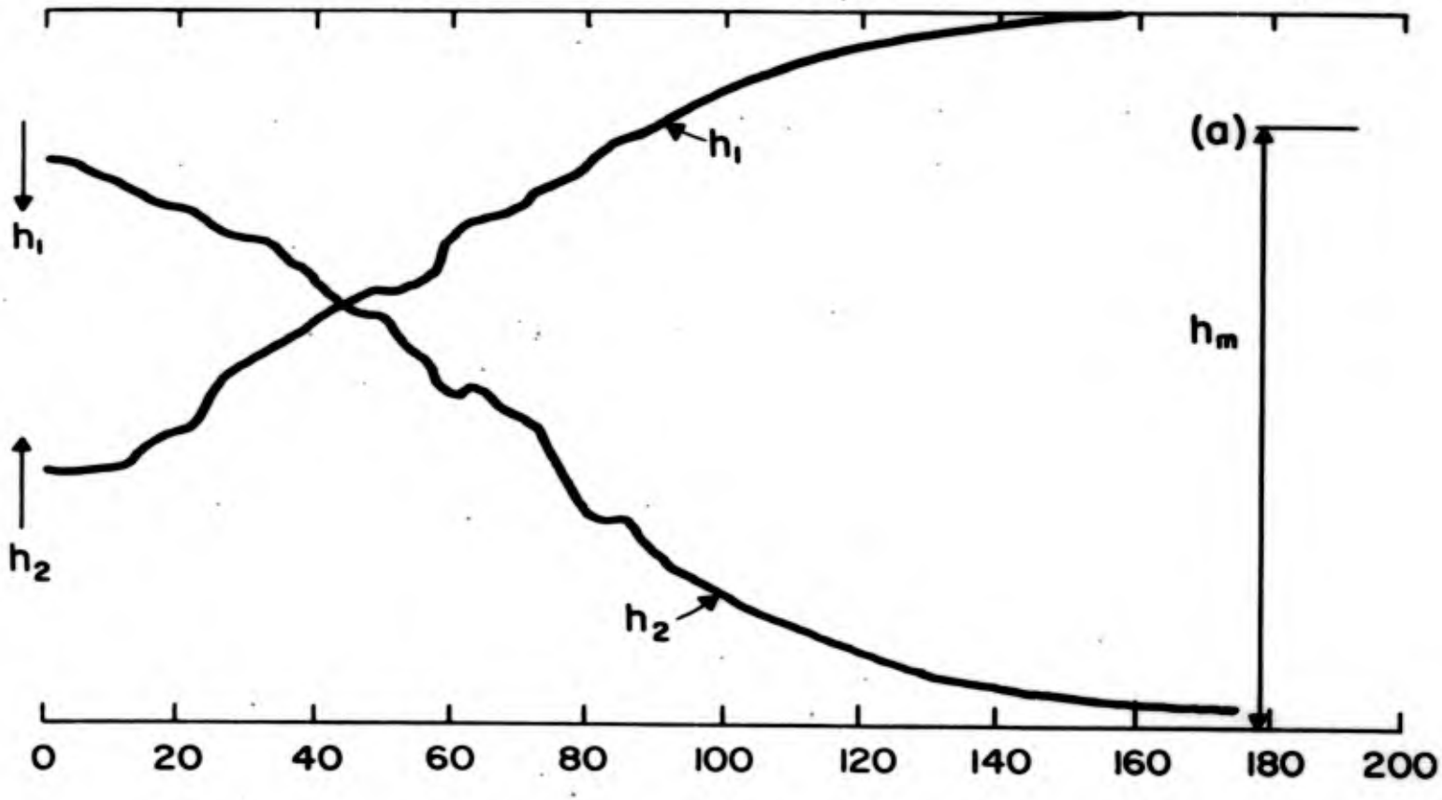

Figure 8. Microwave signal amplitudes h_1 and h_2 from detectors versus time for a decaying plasma in Argon (p 8.3mmHg, 20μ sec/division microwave cut-off pulse height, h_m = 5 division). Time starts with the discharge trigger pulse.

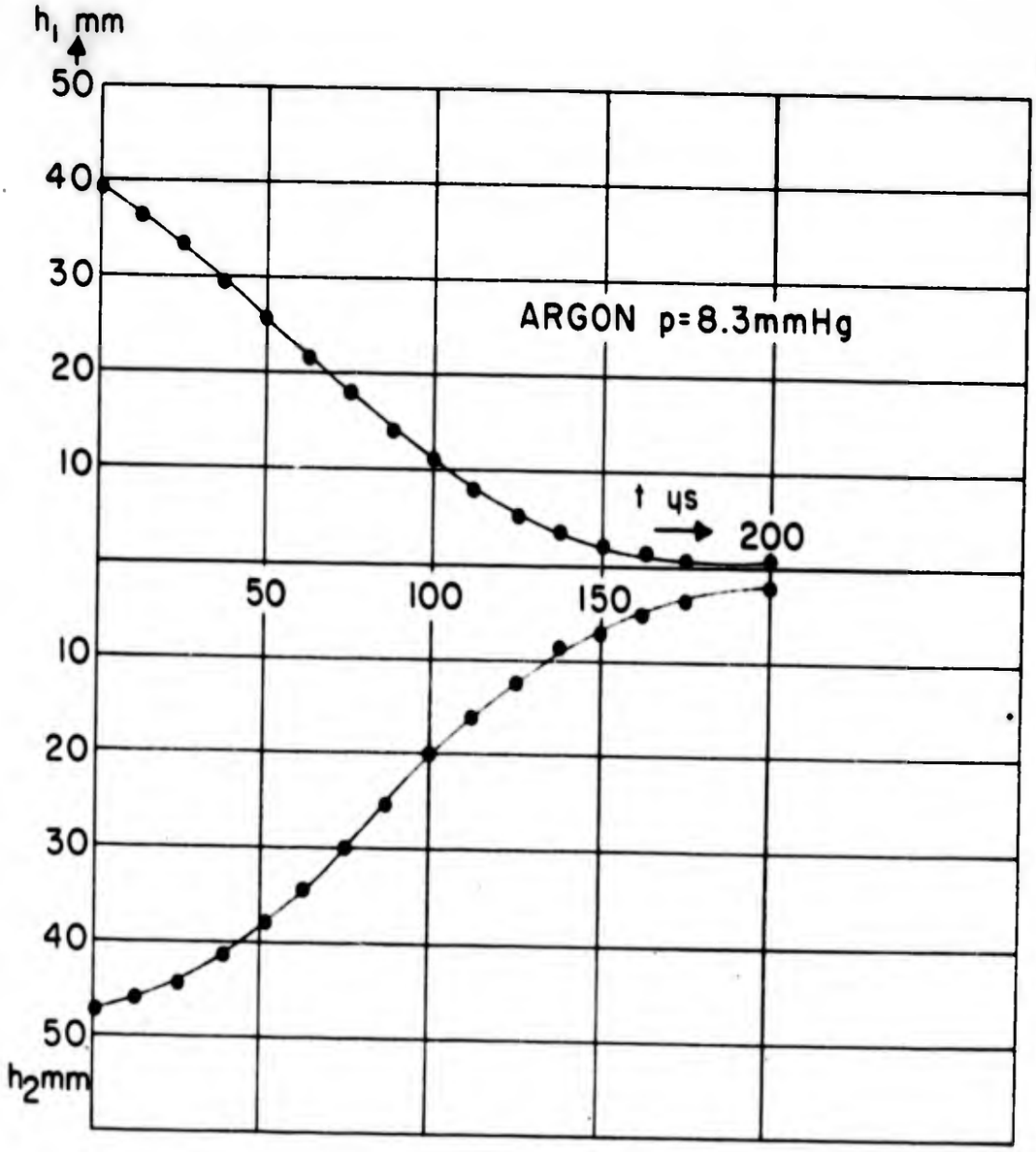

Figure 9. Same as in Figure 8, but smoothened

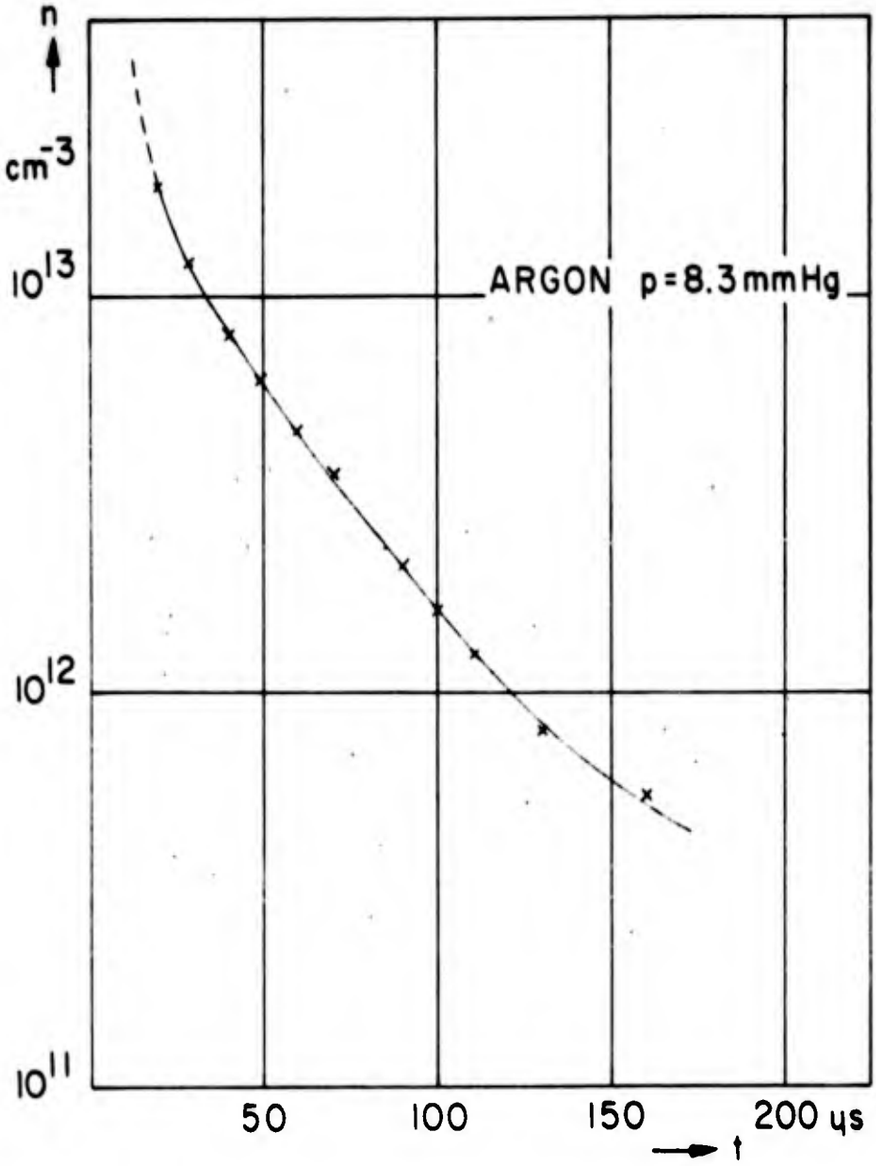

Figure 10. Electron density versus time calculated from Figure 9

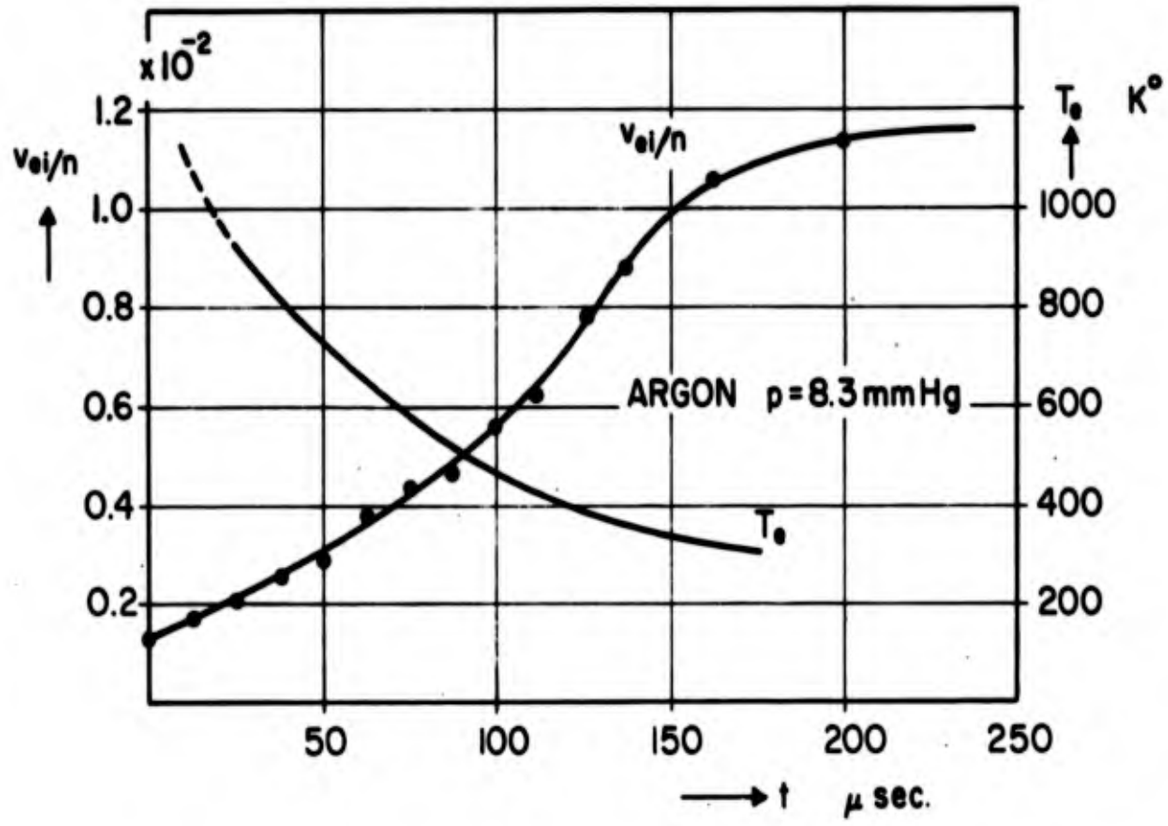

Figure 11. Ratio of the electron-ion collision frequency ν_{ei} to the electron density n, and electron temperature T_e versus time, calculated from Figure 9.

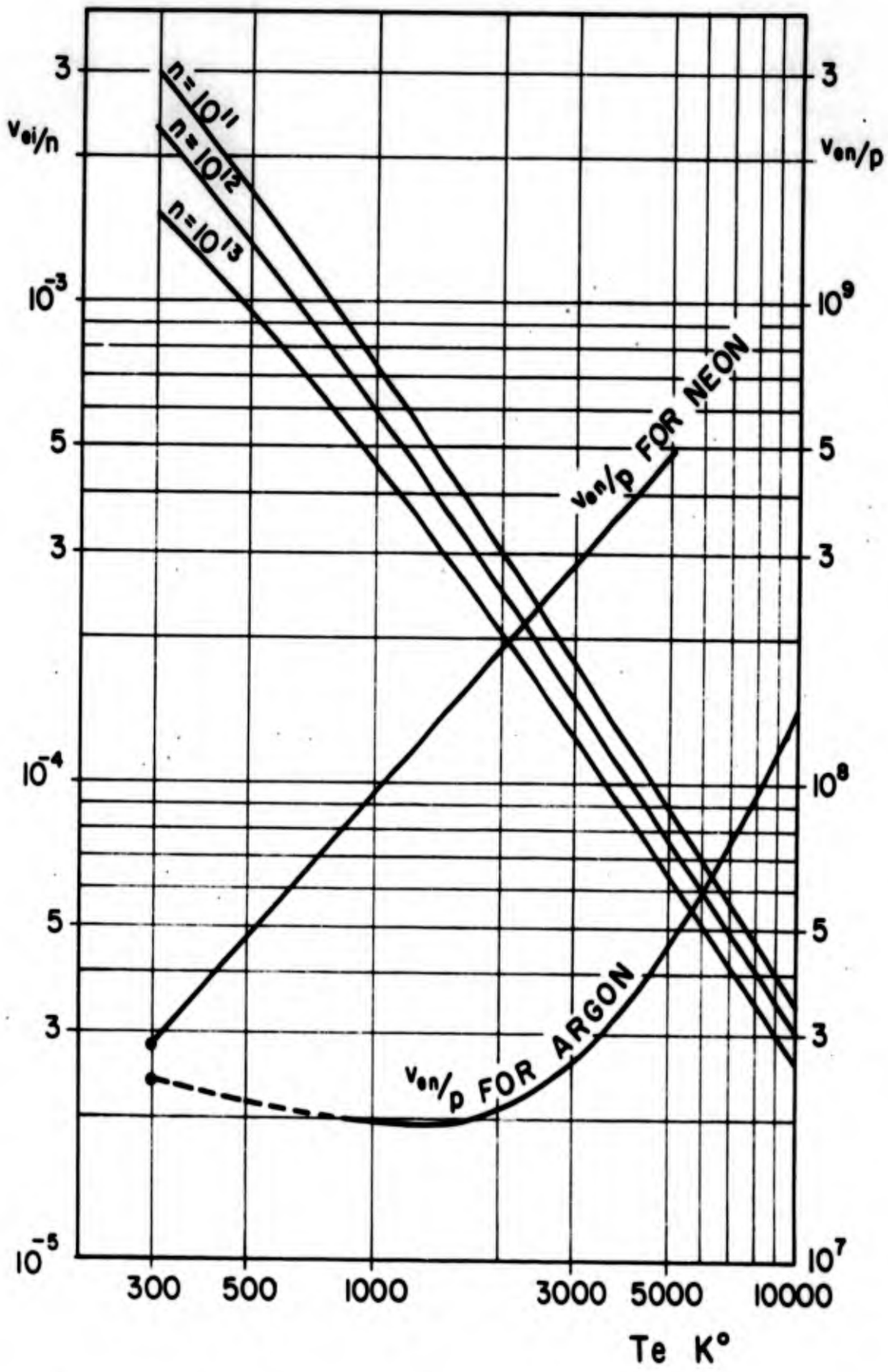

Figure 12. Ratio of the electron-ion collision frequency to the electron density ν_{ei}/n, and ratio of the electron-atom collision frequency to the gas pressure ν_{en}/p for Neon and Argon, versus electron temperature T_e (p in mmHg and n in cm^{-3} are parameters)

By means of a pulse divider the repetition frequency of these discharges is made half of that of the oscilloscope triggering. Therefore, four traces appear simultaneously. A typical oscilloscope trace is shown in Figure 8 where the upper traces (with positive downward deflection) represent the signal picked up by probe 1, now in its minimum position, and the lower traces (positive upward deflection) represent those of probe 2. The two horizontal traces correspond to probe signals 1 and 2 in the absence of plasma. The maximum amplitude of the microwave cut-off pulse is indicated by h_m in trace of probe 2. If probe 1 were at the maximum position (1) h_m would be visible in upper trace too. The axis origin (t = 0) coincides in all the figures with the discharge triggering pulse

Although the origins of the irregularities superimposed on the signals h_1 and h_2 in Figure 8 during the plasma decay are not clearly explained at the present time, these traces were replotted in Figure 9 as smoothed curves, and the electron density and collision frequency are calculated from them with the help of Equations (3) and (5). Figures 10 and 11 show respectively in function of time, the decay of the electron density n and the ratio of the collision frequency ν to the electron density n, during the decay of the plasma

In the range of pressure, density, and temperature of our experiments, the electron-molecule collision frequency ν_{em} can usually be neglected with respect to the electron-ion collision frequency ν_{ei}. The relative importance of these parameters is checked in Figure 12 which plots the theoretical values of ν_{ei}/n and ν_{en}/p [13,14] for Neon and Argon against electron temperature T_e, where p is the pressure in mmHg. Since ν_{ei} is proportional to n and $T_e^{-3/2}$, it is expected that in the late period of the plasma decay as the electron temperature approaches 300^{o}k, the ratio ν_{ei}/n should reach a constant value. Figure 11 shows that the experimental curve approaches the value 1.2×10^{-2} cm^3/sec, which is compared to the theoretical or experimental values of the ratio at room temperature derived by other authors and listed in Table I.

TABLE I

Theoretical and experimental values of $\nu_{ei}/n(cm^{+3}/sec)$ at room temperature

Theory				Experiment			
					(I)	(II)	
Electron Density	Spitzer[15]	Ginsburg[12]	Dougal[16]	Anderson[17]	Dougal[16]		This work
1×10^{11}	3.2×10^{-3}	3.8×10^{-3}	9.6×10^{-3}	3.0×10^{-3}	9.8×10^{-3}	1.2×10^{-2}	1.2×10^{-2} at $n=5\times10^{11}$
1×10^{12}	2.4×10^{-3}	2.9×10^{-3}	5.5×10^{-3}				

(I) Phototube datas of luminous intensity
(II) Microwave interaction
(3),(4) ν_{ei} deduced from τ_{ei}

From the theoretical temperature dependence of the electron-ion collision frequency ν_{ei}, the electron temperature in the decaying plasma is calculated from the measured ν_{ei}/n and plotted in Figure 11. This curve shows, that the electron temperature takes more than 100 μsec to fall from 800°K to 300°K. This time is much longer than expected according to the general equation for the time rate of change of the electron temperature, as follows.

$$-\frac{dT_e}{dt} = \frac{1}{\tau_{ei}}(T_e - T_i) + \frac{1}{\tau_{er}}(T_e - T_g) \qquad (7)$$

where T_e, T_i and T_g are the electron, ion and gas temperatures, respectively, and τ_{ei} and τ_{en} are characteristic times for equi-partition of the temperature between electrons and ions, and electrons and atoms, respectively. τ_{en} is defined as $\tau_{en} = 1/\nu_{en} \cdot M/2m$, where M and m are the atom and electron mass respectively. Similarly, ν_{ei} may be defined as $\tau_{ei} = 1/\nu_{ei} \cdot M_i/2m$, where M_i is the ion mass. The theoretical values of τ_{ei}, derived in different ways, are summarized by Dougal and Goldstein[16]. For Argon at room temperature and for the electron densities met in our experiments (10^{11} - 10^{13} cm^{-3}), τ_{ei}, which is much shorter than τ_{en}, is of the order of a few μsec. One reason which can possibly explain the long electron temperature decay time measured would be the presence of metastable atoms which heat the electron gas by the intermediary of the ion gas.

It was usually assumed that the maximum light intensity originating from the afterglow close to the beginning of a pulsed discharge corresponded to the time when the electron temperature reached 300°k. However, the photomultiplier data of our experiments, especially in Neon afterglow, contradict this assumption since the light intensity maximum appears in less than 20 μsec, whereas the electron temperature does not reach 300°K until more than 100 μsec have elapsed.

In order to check the error in the measurement of n and ν due to the microwave energy lost by radiation through the waveguide hole or along the plasma post, the plasma was replaced by a metal rod of the same diameter. In this case n approaches infinity and it follows from Equation(5,) that x = B and r = 0. Experimentally, r was found to be 0.1 which corresponds to $\nu_{ei}/n = 1.5 \times 10^{-3} cm^3/sec$. Since the highest energy losses are expected at high electron densities, this corresponding value of ν_{ei}/n is thought to be its maximum possible error. It is also probable that the plasma diameter is slightly smaller than the internal tube

diameter, owing to the thin ion sheet usually found close to the wall. This and the possible non-uniformity of the electron distribution due to the proximity of the metallic waveguide may contribute to the measurement error. If the equivalent plasma diameter were known to be smaller, then the constant A in Equations (5) and (5') would increase, partially explaining the high values of ν_{ei}/n found in these experiments. This correction, however, does not affect the calculated electron temperature T_e, since only the -3/2 power of the temperature ratio $\nu_{ei}/n - (T_e/300)^{-3/2}$ is used.

6. COMPRESSING AND HEATING PROCESSES BY SHOCK WAVES

The ratio of the pressure p_2 and gas density ρ_2 behind the shock front to p_1 and ρ_1 in the undisturbed region in front of the shock front ⊙ are known from thermodynamic theory[9],

$$p_2/p_1 = \frac{2rM^2 - (r-1)}{r+1}$$

$$\rho_2/\rho_1 = \frac{M^2(r+1)}{M^2(r+1) + 2} \qquad (8)$$

where M is the Mach number or the ratio of the propagation velocity of the shock wave to the sound velocity in the undisturbed medium and γ is the ratio of the specific heats. From the relation between gas temperature, pressure, and density, $T \sim p/\rho$, the ratio T_2/T_1 of the gas temperature behind and before the shock wave is written as

$$T_2/T_1 = \left\{1 + \frac{M^2(r-1)}{2}\right\}\left\{\frac{4rM^2 - 2(r-1)}{M^2(r+1)^2}\right\} \qquad (9)$$

The undisturbed region referred to above in this experiment is the decaying gaseous plasma. In view of its low degree of ionization and low ion temperature the medium is unaltered for sound wave propagation. Hence the above relations apply. When the medium which is a mixture of three gases, the electron, ion, and neutral gases, is compressed by a propagating, weak, and non-ionizing shock discontinuity, it may be assumed that any constituents of this mixture are compressed in the same ratio, that is $n_2/n_1 \sim \rho_2/\rho_1$, where n_1 and n_2 refer to the electron density in the undisturbed plasma and behind the shock front, respectively.*

---

* Strictly speaking, the ion gas density is first increased by the propagating shock in view of the large collision cross section for momentum transfer of the heavy particles involved. Then, as a consequence of the resulting space charge in the plasma, the increasing electron density follows in a time interval equal to a few plasma oscillations, which is short with respect to the shock-propagation time scale.

This is so if, during the short time compression, the electron and ion losses are negligible. The theoretical value of the rare gas density and temperature ratios n_2/n_1 and T_2/T_1, where $\gamma = 1.67$, are plotted as functions of the Mach number M in Figures 18 and 20.

It is well known that in electrical discharges in gases the electron temperature T_e is generally higher than the ion temperature T_i, which is nearly equal or somewhat higher than the gas temperature T_g. However, in an already weakly ionized gas, the passage of a weak shock wave heats the neutral atoms and the ion gases more efficiently than the electrons. As a result,

$$T_e \leq T_g \text{ or } T_i \tag{10}$$

The time rate of change of the electron temperature increase in this case is described by the following equation

$$\frac{dT_e}{dt} = \frac{1}{\tau_{ei}} (T_i - T_e) + \frac{1}{\tau_{ei}} (T_g - T_e) + K \nabla^2 T_e \tag{11}$$

where K is a coefficient due to thermal conduction. Then Equation(11) and the relation $n_2/n_1 \quad \rho_2/\rho_1$ show that when the gas is heated by the shock wave, the electron density immediately follows the gas density increase, while the electron temperature reaches its maximum value with some delay.

In Figure 13 the ionization degree is shown for different gases. ($U_i = 5eV$ is the case for an impurity).

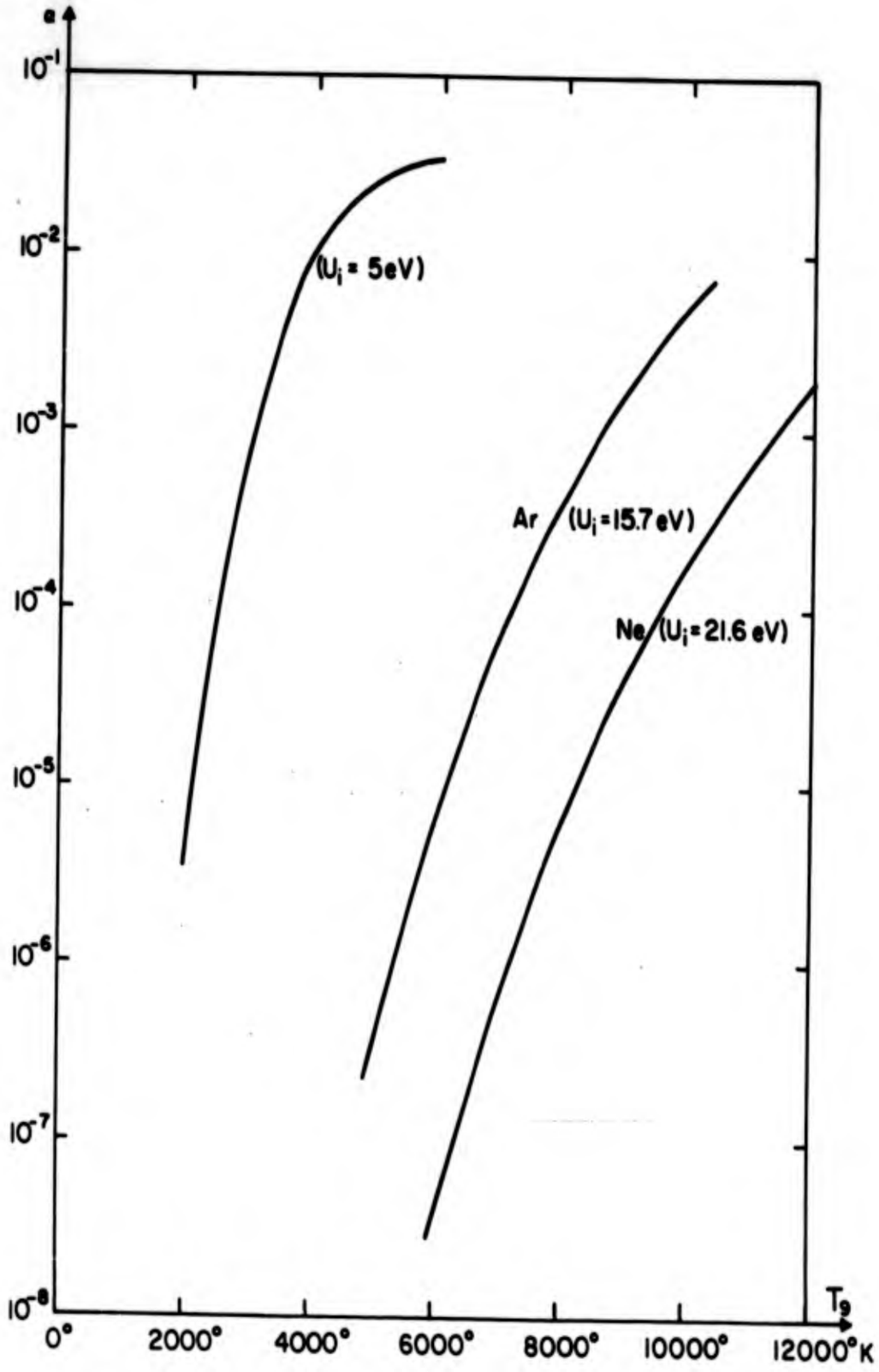

Figure 13. Ionization degree α versus electron temperature T_e for different ionization potentials

7. EXPERIMENTAL RESULTS

At first the shock propagation velocity was measured by using the probes 2 and 3. The lower trace in Figure 14 shows the signal from the first waveguide. There are two noticeable discontinuities in each trace: the first one, denoted by (a), is due to the shock wave, the second, (b) is thought to correspond to the plasma expanding from the condenser discharge region. Without pre-ionization, (a) disappears because the relatively weak shock wave does not produce enough electrons to be detected by the microwave method described here. The discontinuity (b) appears clearly even without any pre-ionization but rapidly decreases in both magnitude and velocity as the distance from the origin is increased.

For the arrival times t_1 and t_2 of the peak (a) at the first and the second waveguides and for distances $d_1 = 23.5$ cm and $d_2 = 29.5$ cm, a value of the exponent β in Equation(1)was found to be 0.47 ± 0.02 in Neon gas. The pressure and the condenser voltage ranged, respectively, from 4 to 13 mm Hg and 3 to 7 kv. The local shock velocity (Mach number) at the level of the waveguide then can be easily calculated from the measured mean velocity (d_1/t_1) and β.

The plasma background for weak shock wave propagation studies by microwaves is also useful in another way. Indeed, the decaying plasma gives rise to an afterglow which can be observed by means of a photomultiplier at any position along the tube and in the waveguide in particular. In the course of the shock propagation in the plasma, the afterglow must be altered. Hence, optical observations on the afterglow, correlated with microwave measurements, provide an additional means of investigations in these studies, as illustrated in Figure 15. However, when the condenser discharge giving rise to the shock wave is produced between electrodes A and B in Figure 4, a small discharge current is also flowing simultaneously between electrodes A and C. This stray current enhances the pre-ionization and the associated afterglow is shown in Figure 15 trace (II). The light intensity and the microwave signal in another case are simultaneously displayed in Figure 16. For a very intense condenser discharge, the intensity of this visible, enhanced afterglow may be such that the discontinuity in this light intensity, produced by the propagating, weak shock wave illustrated by (a) in Figure 15 becomes difficult to observe.

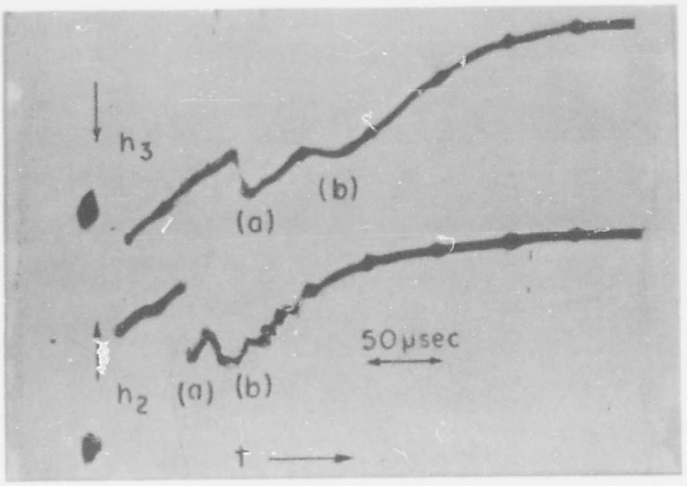

Figure 14. Microwave signal amplitudes h_1 and h_2 versus time from the first and second waveguides 50 μsec/division Ne, p = 5.8 mm Hg, 5 kv, 8 μF

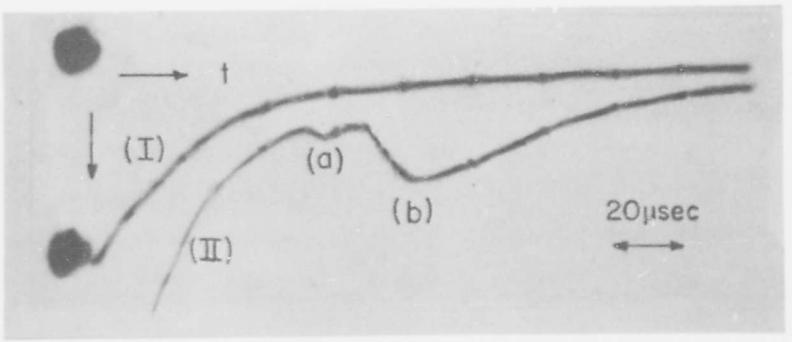

Figure 15. Light signal versus time. (I): with pre-ionization (II): condenser discharge and pre-ionization, 50 μsec/division, Ne, p = 4.5 mm Hg, 5 kv, 8 μsec (Light intensity in arbitrary units)

The visible afterglow is generally attributed to recombination of electrons and positive ions or decaying plasmas. The discontinuity in the visible light of this afterglow at any one time and space position in the shock tube may probably be attributed to the alteration of the recombination procedure by the weak shock discontinuity. It is known that the light intensity of recombination, which is proportional to the number densities of the recombining charge and the recombination coefficient is dependent upon the relative velocities (temperatures) of these charges. Hence a sudden variation either in the densities of the recombining charges or in their temperature should bring about a change in the visible light intensity. However, the effect on the light intensity of an increase in densities is opposite to the effect due to an increase in temperatures, because the recombination coefficient decreases with increasing temperatures. As a result of these compensating effects, the discontinuity in the visible afterglow due to shock waves may be small. The enhanced visible intensity in the afterglow, indicated by (b) in Figures 15 and 16 is again thought to be related to the expanding plasma following the shock discontinuity.

Next, the electron densities n_2 and n_1 across the shock front was calculated from the photographically recorded traces of the two microwave signals detected by the two probes 1 and 2. Figures 17(A) and (B) show examples of the signals h_1 and h_2. The ratio of the electron densities n_2/n_1 is calculated and plotted versus Mach number in Figure 18 (crosses). For comparison, the theoretically predicted ratio of gas densities ρ_2/ρ_1 as a function of Mach number is also shown in the figure (solid line). It is apparent that the variation of the ratio of electron densities across the shock discontinuity as a function of shock velocity is quite similar to the variation of the gas densities. Therefore, it appears reasonable to assume that the electron density increase, due to a weak shock wave propagating in such plasmas, is a consequence of the compression of the weakly ionized gas. The possible discrepancy in the range of small Mach number (1 to 2) is likely due to the duration of the compression, which is then comparable to or longer than the characteristic time for recombination and/or diffusion losses of electrons. In the plasma considered, since the electron-atom collision frequency ν_{en} for momentum transfer is negligibly smaller than the electron-ion collision frequency ν_{ei} in the temperature range involved, the electron temperature is obtained from the electron temperature dependence.

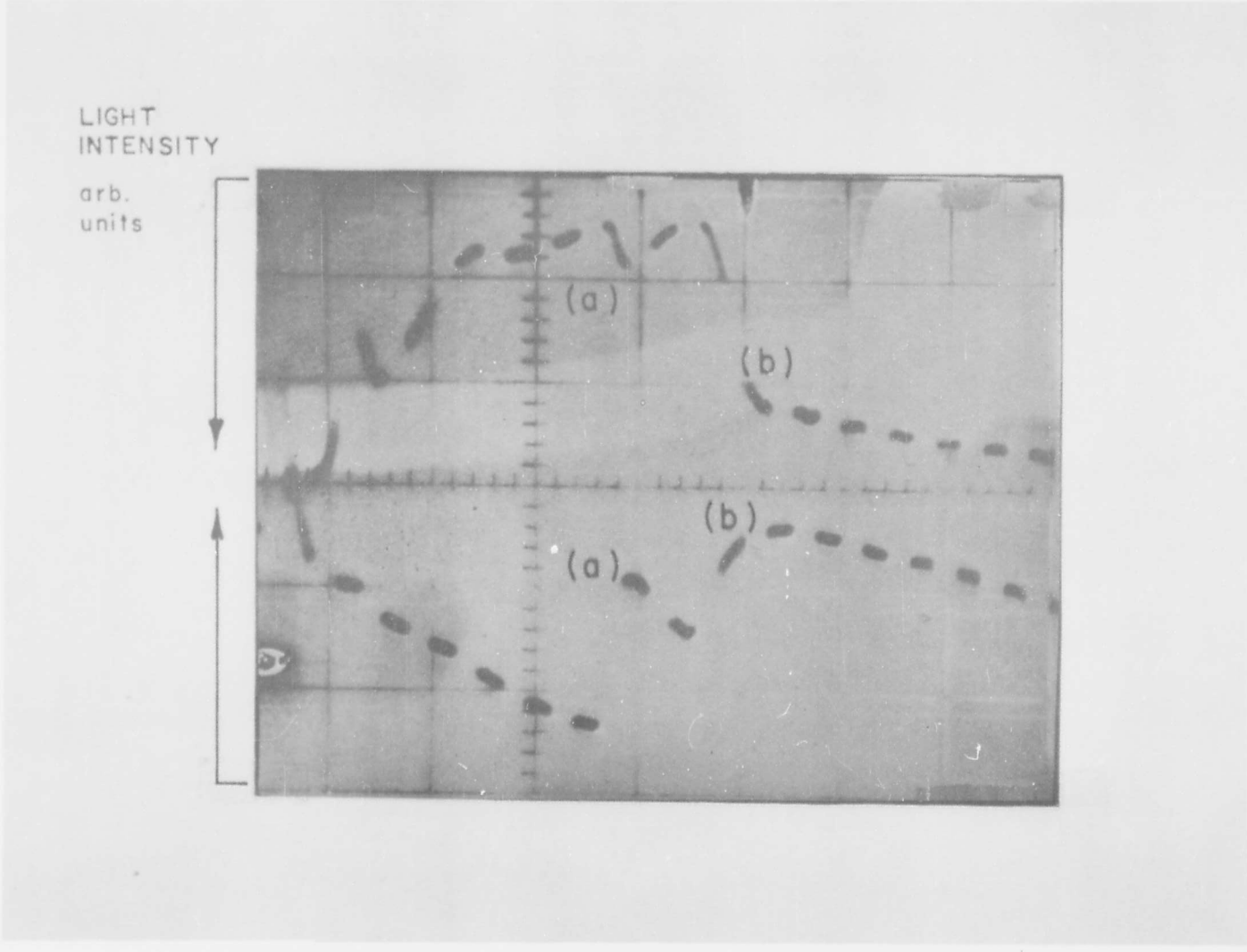

Figure 16. Simultaneous recording of light intensity (upper trace) and microwave signal h_1 (lower trace)

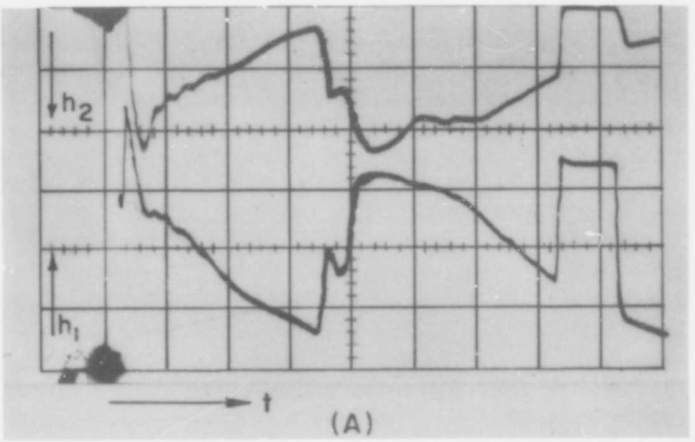

Ne, p = 4.1 mm Hg, 4.3 kv

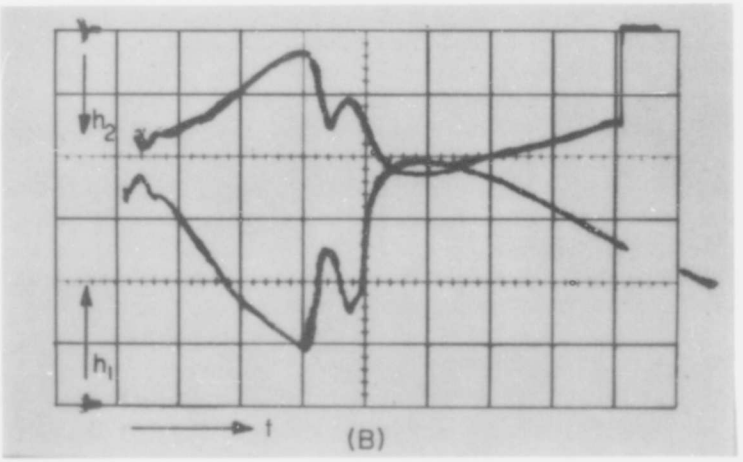

Ne, p = 7.6 mm Hg, 4.5 kv

Figure 17. Microwave signals h_1 and h_2 versus time in the shock wave experiments, 20 μsec/division, 8 μF.

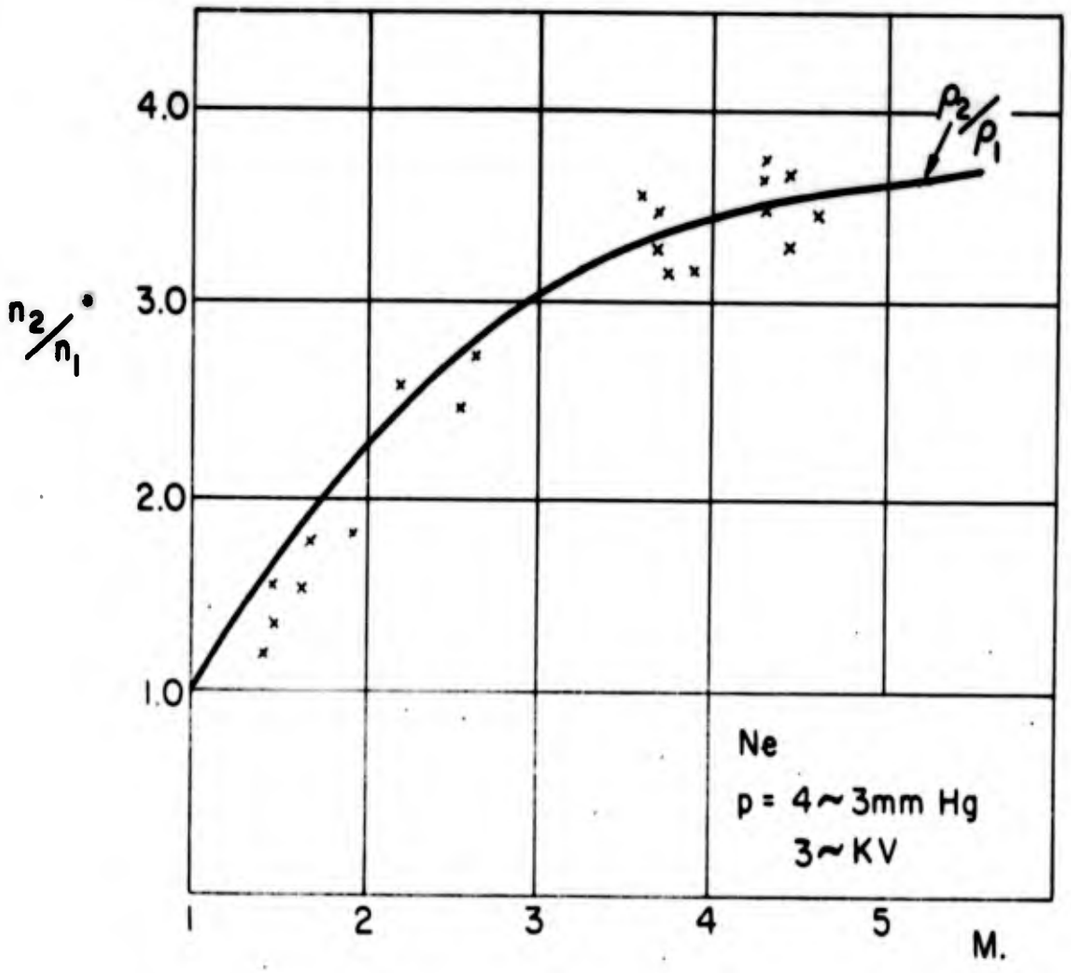

Figure 18. Comparison between the gas density ratio ρ_2/ρ_1, calculated from Mach no., and the measured electron density ratio, n_2/n_1, Ne, p = 4-13mmHg

From the recorded microwave probe signals illustrated in Figure 19(A), the variation of the electron density and the electron temperature of the plasma in the presence of a propagating shock wave is computed and plotted in Figure 19(B). Another example of such electron density and electron temperature variation due to weak shock waves propagated in plasmas under different conditions is seen in Figure 19(C). It is seen on these figures that the electron temperature does not reach its maximum at the same time as the electron density. Since the energy from the propagating shock wave is transferred very efficiently only to the ions, the electron gas should be heated by the warm gas of the ions. This process proceeds with a rather long time constant τ_{ei}, resulting in a delay in the temperature rise of the electron gas. This delay is obviously shorter for shocks of higher Mach number. These observations appear to justify the assumption made in Equation(11). Although no delay was expected in the electron density rise due to compression, some was observed. The observed rate of electron density increase may depend upon the shape of the shock discontinuity and the length of the shock tube within the waveguide, which in these experiments was 4 mm. Figure 20 compares the theoretical neutral gas temperature behind the shock front (upper line) calculated from the measured Mach number by Equation 9 to the measured corresponding electron temperature, where both temperatures are normalized to 300^{o}K.

The shock velocity (Mach number) increases with decreasing gas pressure and increasing condenser voltage. It is observed that in addition to an enhanced shock velocity, in particular at lower gas pressures, the time separation of the discontinuities (a) and (b) (Figure 19(A)) of the microwave signals is shortened. This indicates an increase in the velocity of the expanding initially highly ionized gas which causes (b).

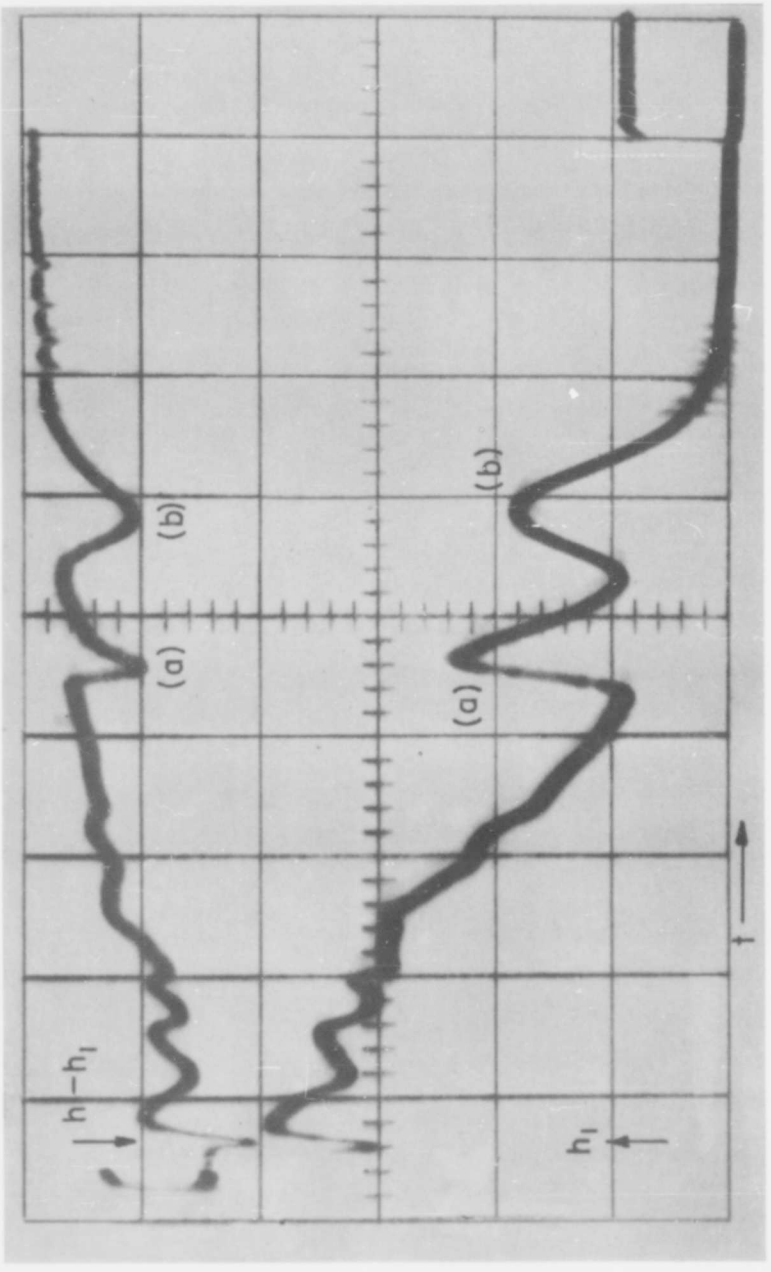

Figure 19(A). Microwave signal amplitude h_1 and h_2-h_1 versus time, 20 μsec/division, Argon, p = 12 mm Hg, 5 kv, 8 μF

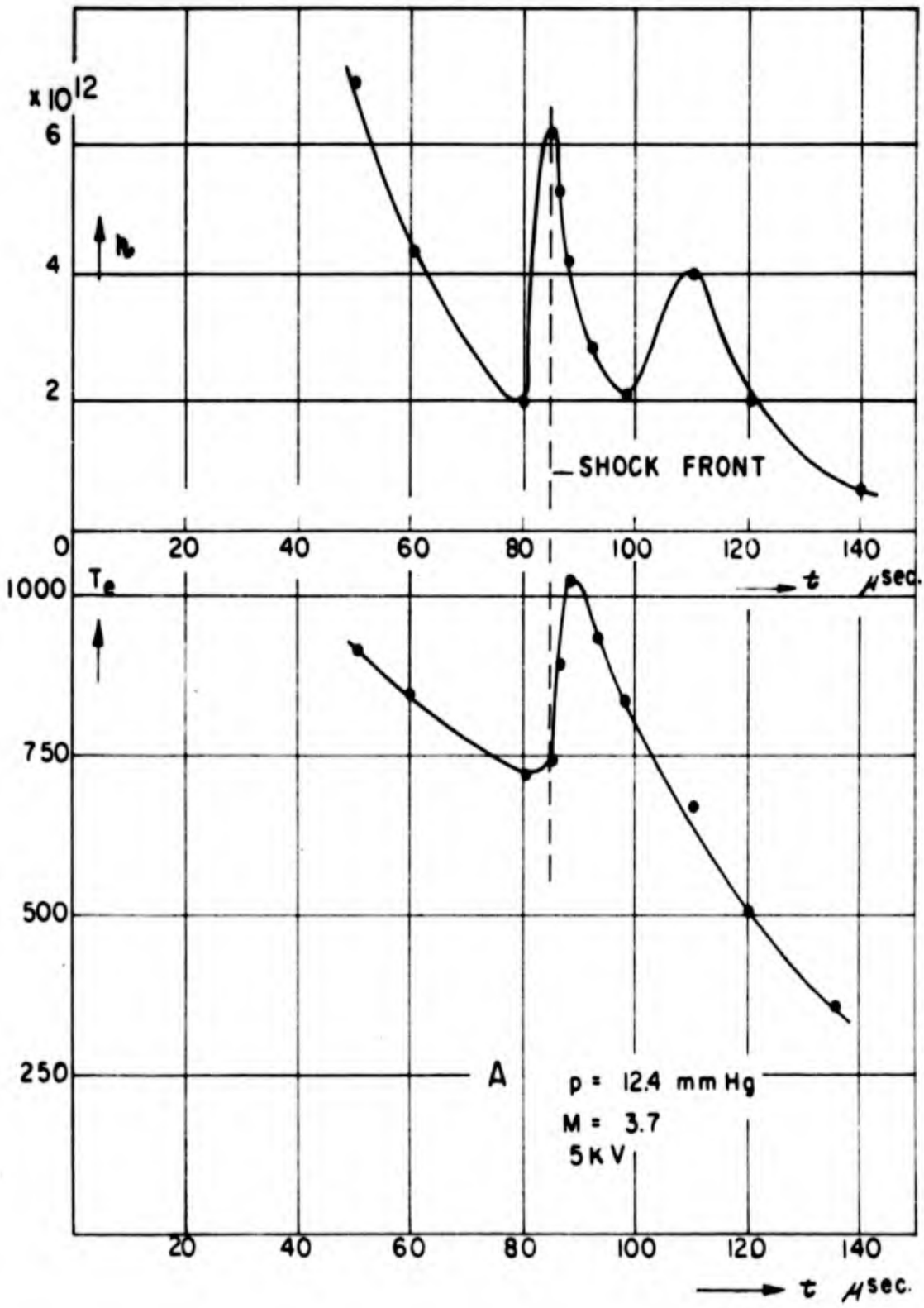

Figure 19(B). Changes in the electron density and the electron temperature versus time, calculated from (A)

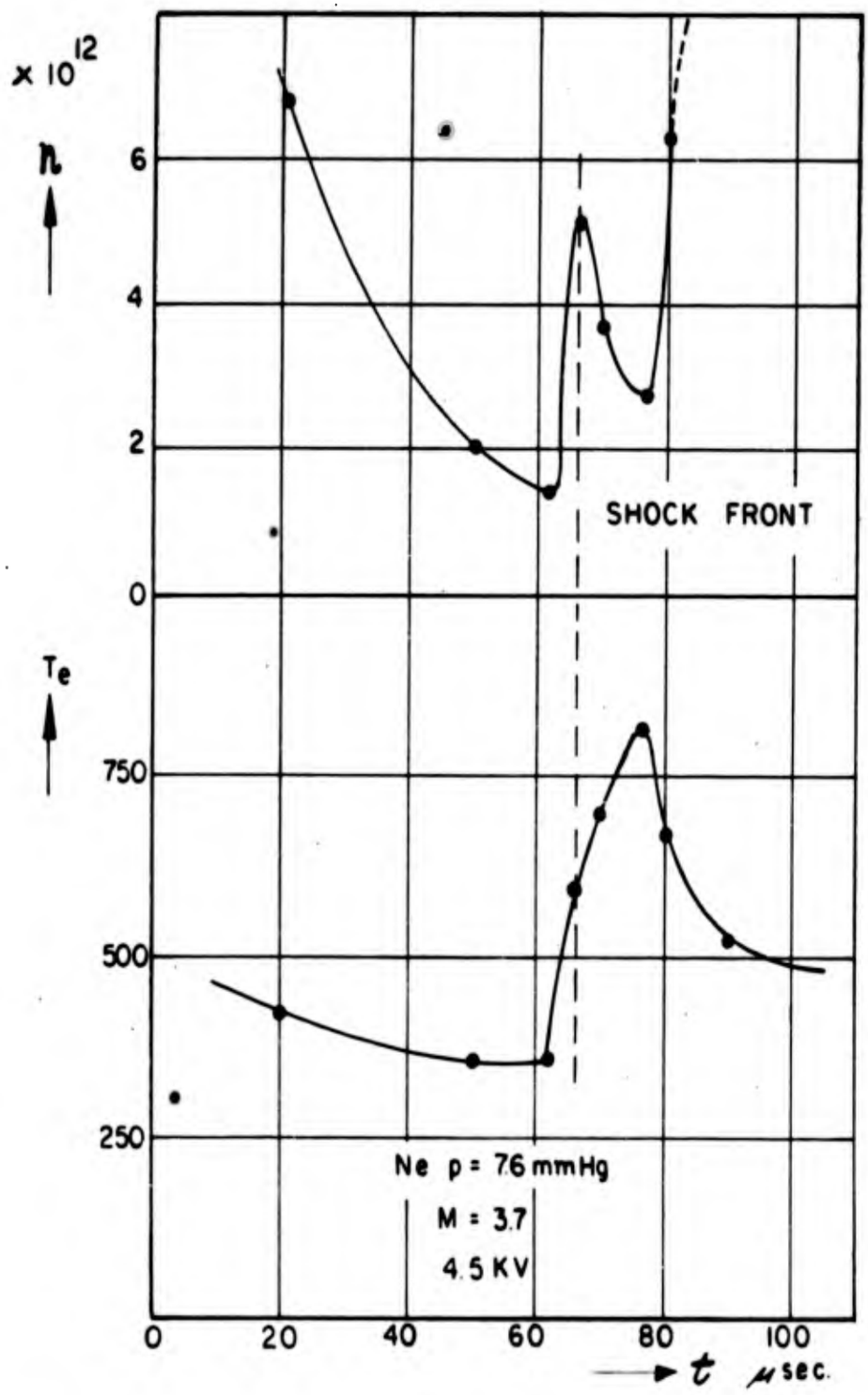

Figure 19(C). Same as Figure (B), but for p = 7.6mmHg, 4.5kv, 8μF

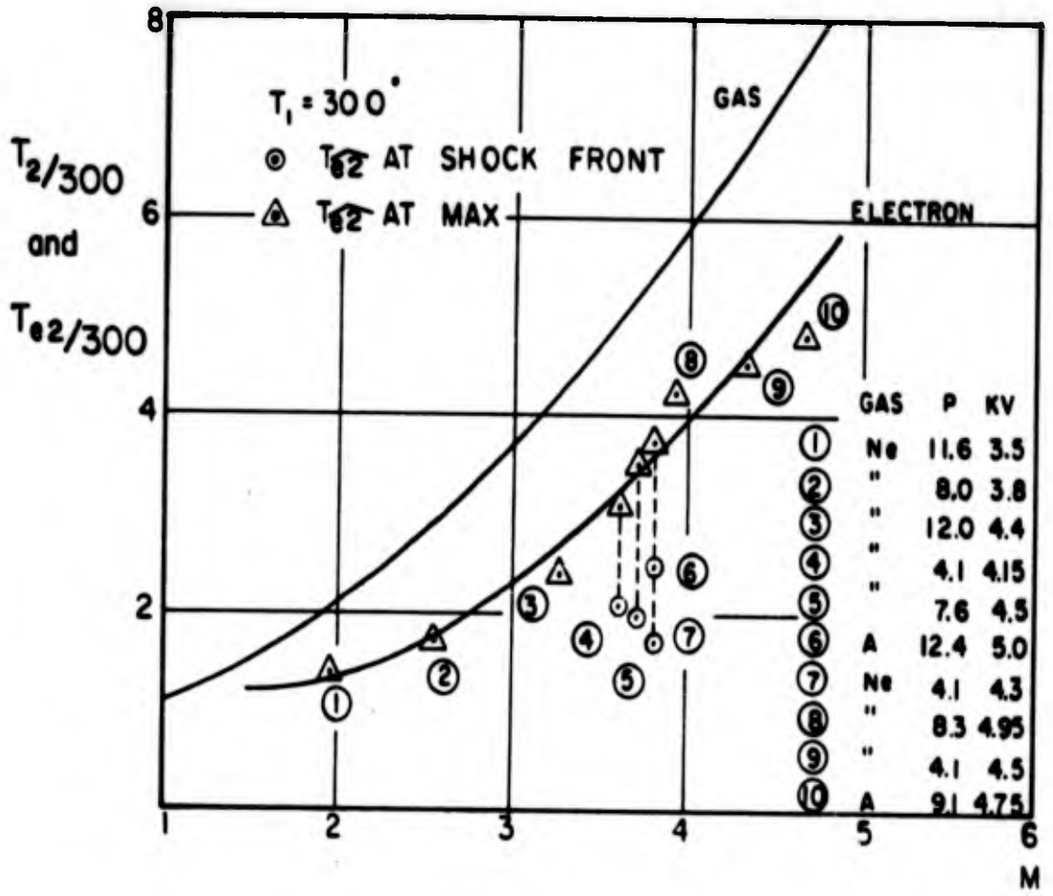

Figure 20. Comparison of the neutral gas temperature calculated from the Mach no., to the electron temperature behind the shock, where both temperatures are normalized to $300^{\circ}K$.

8. SUMMARY AND CONCLUSIONS

The method described above, which is based on the known interaction of low-level microwaves with free electrons in weakly ionized low pressure gases at relatively low temperatures, has proved to be a convenient one for the study of non-ionizing shock waves. The main shock characteristics which are accessible to direct determination are the instantaneous and average velocities of shock discontinuities propagated in low pressure and low temperature ($T_e \sim 300^{\circ}K$) weakly ionized gases. Associated with the change in shock propagation velocities, the exchange between the propagating shock discontinuities and the ionized gaseous medium is studied in some detail through the intermediary of the electron gas. Indeed, as known from previous plasma studies the electron gas of the plasma interacts strongly with both the charged (and the neutral), heavy particles of the background plasma with which the propagating shock wave exchanges energy with great efficiency.

In addition to the electro-magnetic behavior the optical properties of the background plasma also contributed to these studies. Since the light emitted by the plasma is dependent upon the energy state (or temperature) of the electron gas in the plasma, any change of the energy state of the electrons brought about, in particular, by the propagating shock wave provides us with an independent but complementary means of observation, which is directly correlated to the microwave measurements.

While the microwave measurements described in this paper are only in the X-band (~9000mc), the method is not limited to this frequency band. The best appropriate microwave frequencies for these studies being generally determined by geometrical considerations. Similarly, the pressure and degree of ionization of the background gases to be used for weak shock wave propagation studies are not limited to the cases reported here.

PART II

A PROPOSED MICROWAVE REFLECTION METHOD FOR THE STUDY OF HIGH ENERGY SHOCK WAVE PRODUCED HIGH DENSITY PLASMAS

by

S. Takeda

M. Roux

9. CALCULATION OF THE REFLECTION COEFFICIENT

In the high Mach number region it is difficult to carry out shock-wave experiments by means of microwave techniques because such techniques are restriced when high electron densities are encountered. In this section we describe a new method for measuring high electron densities in plasmas.

The well known method for measuring the electron density by means of an electromagnetic wave is based on the fact that the complex conductivity of the medium to be measured depends on the electrons density and the collision frequency. When the frequency of the electromagnetic wave is much lower than the plasma frequency, most of the energy of the incident wave cannot penetrate deeply into the plasma and is reflected at the "surface" of the plasma. However, the reflection at the surface of a high electron density plasma is a little different from that at a perfect conductor.

In the complex reflection coefficient, given by $|R|\, e^{j\theta}$, a perfect conductor shows $|R| = 1$ and $\theta = 180^{o}$. Therefore, in principle the measurement of the small deviations, $1 - |R|$ and $180^{o} - \theta = \phi$ should enable one to determine the electron densities corresponding to frequencies much higher than the wave frequency, at least within the penetrated skin of the plasma.

A plane electromagnetic wave, propagating through a plasma with a complex conductivity σ, takes the form $\exp j(\omega t - kz)$, where k, the propagation constant in the medium, is given by the expression,

$$k = \alpha - j\beta = k_{o}\left(1 - j\frac{\sigma}{\omega\varepsilon}\right) \tag{12}$$

where k_{o} is the phase constant in a vacuum; an approximate expression of the complex conductivity σ of the plasma, as well-known, is

$$\sigma = \frac{ne^{2}}{m}\ \frac{1}{\nu + j\omega} \tag{13}$$

From Equations 1 and 2 and making use of the relation $ne^{2}/m\varepsilon\omega^{2} = \omega_{p}{}^{2}/\omega^{2}$, one obtains

$$\alpha^2 = \frac{k_o^2}{2}\left[\left\{1 - \frac{\omega_p^2/\omega^2}{1 + (\nu/\omega)^2}\right\} + \left\{\left(1 - \frac{\omega_p^2/\omega^2}{1 + (\nu/\omega)^2}\right)^2 + (\nu/\omega)^2\left(\frac{\omega_p^2/\omega^2}{1 + (\nu/\omega)^2}\right)^2\right\}^{1/2}\right] \tag{14a}$$

$$\beta^2 = \frac{h_o}{2}\left[-\left\{1 - \frac{\omega_p^2/\omega^2}{1 + (\nu/\omega)^2}\right\} + \left\{\left(1 - \frac{\omega_p^2/\omega^2}{1 + (\nu/\omega)^2}\right)^2 + (\nu/\omega)^2\left(\frac{\omega_p^2/\omega^2}{1+(\nu/\omega)^2}\right)^2\right\}^{1/2}\right] \tag{14b}$$

The absolute value of the reflection coefficient R, and its phase angle θ are given by:

$$\left|R\right| = \left|\frac{k_o - k}{k_o + k}\right| = \left\{\frac{(k_o^2 - \alpha^2 - \beta^2)^2 + 4k_o^2\beta^2}{(k_o + \alpha)^2 + \beta^2}\right\}^{1/2} \tag{15a}$$

$$\tan\theta = -\tan\phi = \frac{2k_o\beta}{k_o^2 - \alpha^2 - \beta^2} \tag{15b}$$

if

$$\nu/\omega = 0$$

$$\tan\phi = \frac{2\sqrt{\omega_p^2/\omega^2 - 1}}{\omega_p^2/\omega^2 - 2}\ , \quad \left|R\right| = 1 \tag{15b'}$$

When $(\omega_p/\omega)^2/1 + (\nu/\omega)^2 \gg 1$, α and β simplify to:

$$\alpha^2 = \frac{k_o^2}{2}\ \frac{\omega_p^2/\omega^2}{1 + (\nu/\omega)^2}\left[\left\{1 + (\nu/\omega)^2\right\}^{1/2} - 1\right] \tag{14c}$$

$$\beta^2 = \frac{k_o^2}{2}\ \frac{\omega_p^2/\omega^2}{1 + (\nu/\omega)^2}\left[\left\{1 + (\nu/\omega)^2\right\}^{1/2} + 1\right] \tag{14d}$$

Equations (15a) and (15b) can be rewritten as,

$$|R| = \frac{\left\{(1-C)^2 + B^2\right\}^{1/2}}{1 + A + BC}$$

$$1 - |R| = A - \frac{B^2}{2} + 2C \qquad (15c)$$

$$\tan \phi = \frac{B}{1-C}$$

where

$$A = \frac{2\alpha k_o}{\alpha^2 + \beta^2} = \frac{\sqrt{2}\left[\left\{1 + (\nu/\omega)^2\right\}^{1/2} - 1\right]^{1/2}}{(\omega_p/\omega)}$$

$$B = \frac{2\beta k_o}{\alpha^2+\beta^2} = \frac{\sqrt{2}\left[\left\{1 + (\nu/\omega)^2\right\}^{1/2} + 1\right]^{1/2}}{(\omega_p/\omega)}$$

$$C = \frac{k_o^2}{\alpha^2+\beta^2} = \frac{\left\{1 + (\nu/\omega)^2\right\}^{1/2}}{\omega_p/\omega}$$

Again, when $(\omega_p/\omega)^2/1 + (\nu/\omega)^2 \gg 1$, (15c) and (15d) simplify to

$$1 - |R| = A = \frac{\sqrt{2}}{\omega_p/\omega}\left[\left\{1 + (\nu/\omega)^2\right\}^{1/2} - 1\right]^{1/2} \qquad (15e)$$

$$\tan \phi = B = \frac{\sqrt{2}}{\omega_p/\omega}\left[\left\{1 + (\nu/\omega)^2\right\}^{1/2} + 1\right]^{1/2} \qquad (15f)$$

The values if $\tan \phi$, ϕ and $1 - |R|$ versus ω_p^2/ω^2, using these formulas, are shown in Figure 21, 22 and 23 for different values of the parameter ν/ω. For $\omega_p^2/\omega^2 \geq 2$, the value of $\tan \phi$ for $\nu/\omega < 1$ does not differ too much from its value for $\nu/\omega = 0$. However, as shown in Figure 22, deviates markedly from the case $\nu/\omega = 0$, when $\omega_p^2/\omega^2 < 2$. Solving Equations (15e) and (15f) for

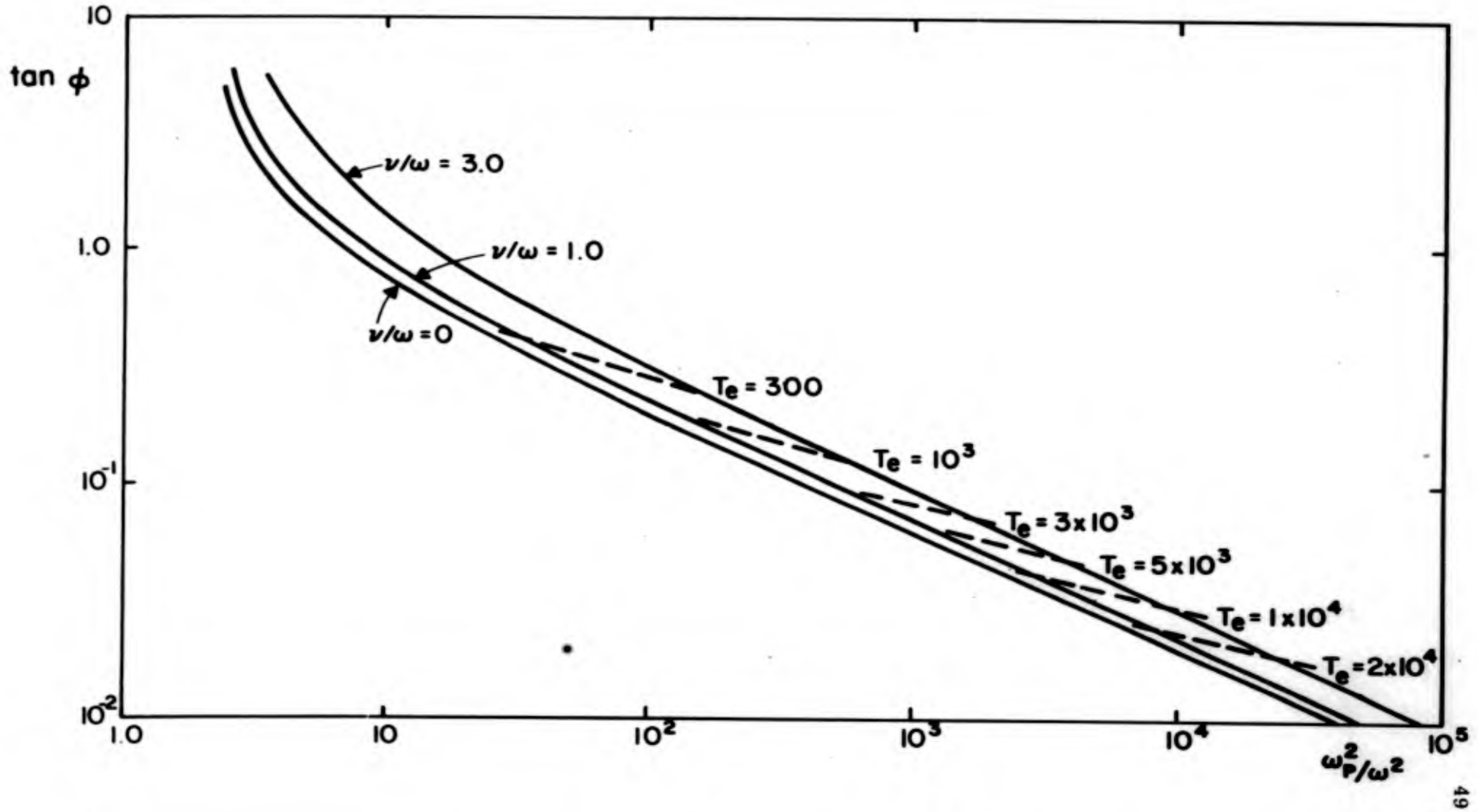

Figure 21. Relation of tan φ versus ω_p^2/ω^2 for different values of ν/ω

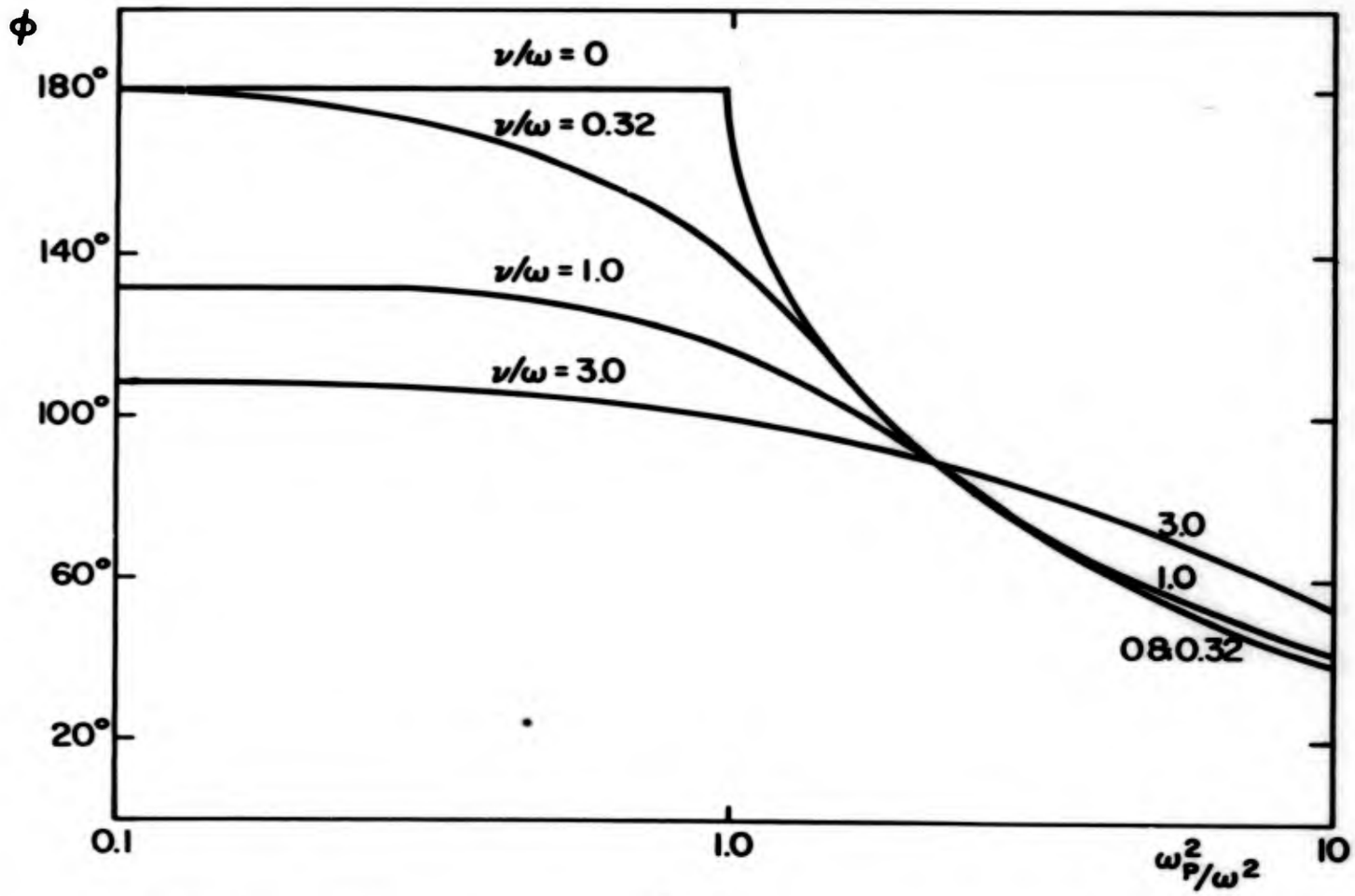

Figure 22. Relation of φ versus ω_p^2/ω^2 for different values of ν/ω ($\omega_p^2/\omega^2 = 0.1 \sim 10$)

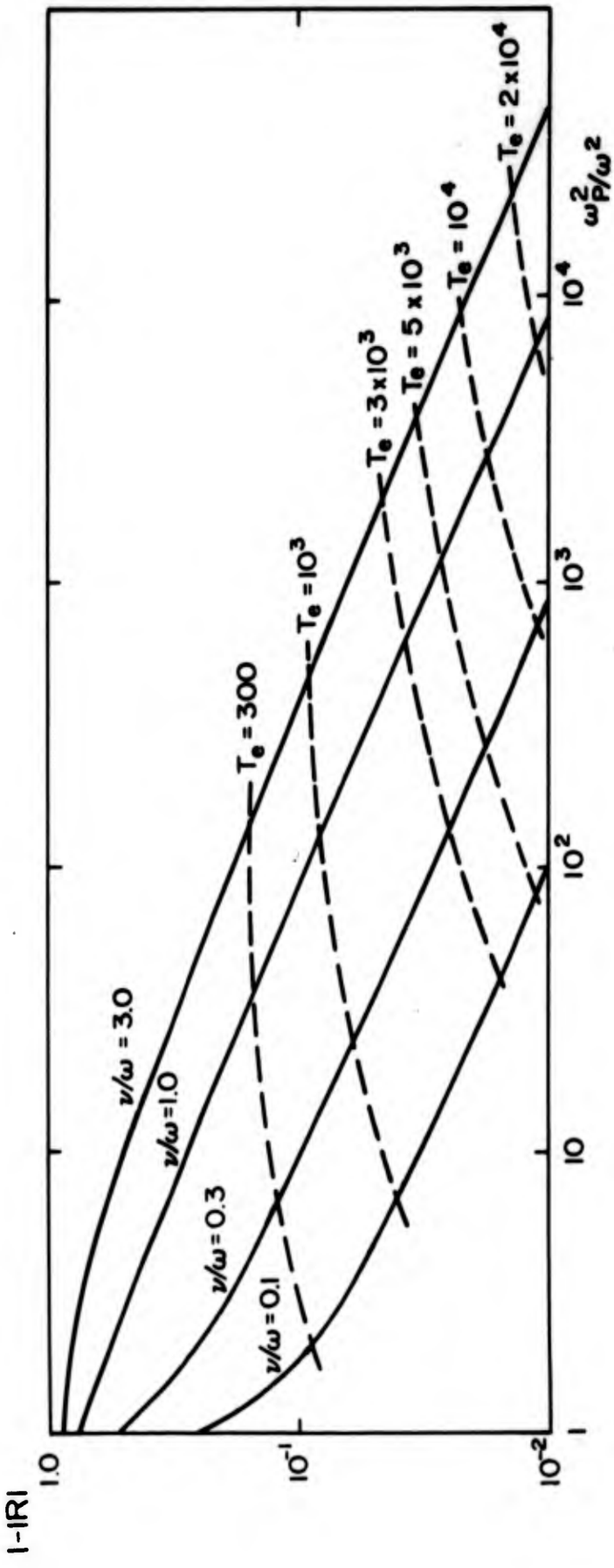

Figure 23. Relation of 1 - |R| versus ω_p^2/ω^2 for different values of ν/ω

ω_p^2/ω^2 and $(\nu/\omega)^2$,

$$\omega_p^2/\omega^2 = \frac{4}{\tan^2\phi - (1-|R|)^2} \tag{16a}$$

$$(\nu/\omega)^2 = \left[\frac{1 + \frac{\left\{1-|R|\right\}^2}{\tan^2\phi}}{1 - \frac{\left\{1-|R|\right\}^2}{\tan^2\phi}}\right]^2 - 1 \tag{16b}$$

and when $\nu/\omega \ll 1$

$$1 - |R| = 0 \tag{16c}$$

and

$$\frac{\omega_p^2}{\omega^2} = \frac{4}{\tan^2\phi} \tag{16d}$$

It may be worthwhile to note that $\phi = 11^\circ$ at $\omega_p^2/\omega^2 = 10^2$ for $\nu/\omega = 0$. This means that $n = 10^{14}$ cm^{-3} will be very easily measured by using a wave at 9000 mc.

The electromagnetic wave is very rapidly attenuated in plasmas in which ω_p^2/ω^2 is greater than one. The attenuation distance d is defined[19] by

$$d = 1/\beta \tag{17}$$

The ratio of the attenuation distance to the free space wave length d/λ is shown in Figure 24 for different ν/ω. From (14b) it is simplified for $\nu/\omega = 0$, as

$$\frac{d}{\lambda} = \frac{1}{2\pi} \frac{1}{\left\{(\omega_p/\omega)^2 - 1\right\}^{1/2}} \tag{18}$$

Except at the low values of ω_p/ω, this ratio is very small. A plasma which has a thickness larger than this value is considered to be infinite. For a plasma in a glass tube, the electron density in the near vicinity of the glass wall may not be uniform, but may change rapidly within a distance which is in order of the

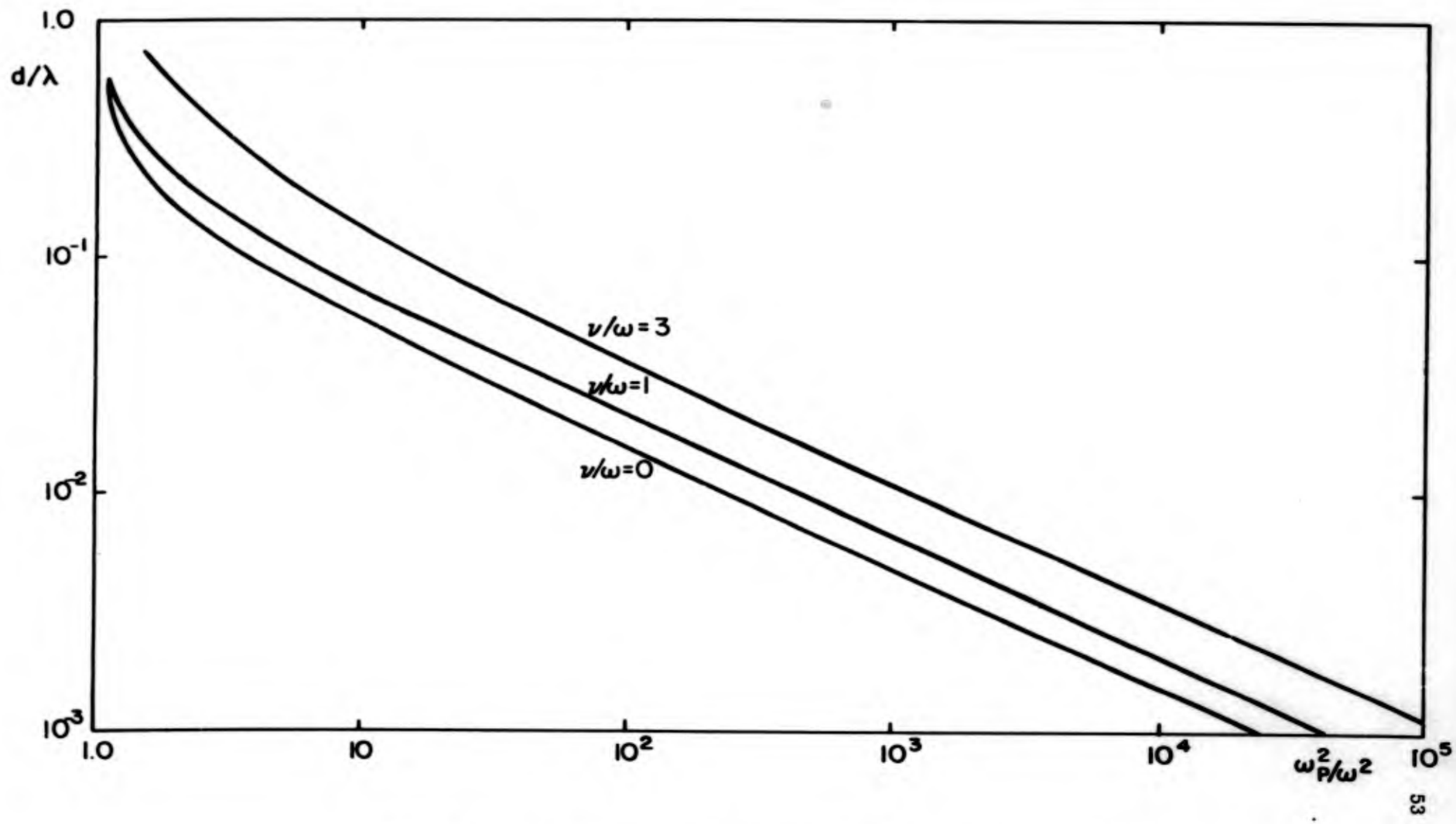

Figure 24. Relation of d/λ versus ω_p^2/ω^2 for different values of ν/ω

the Debye length. The latter, at high enough electron density, is much smaller than the attenuation distance. Therefore, this non-uniformity can be neglected.

The next problem is the measurement of the small values of $1 - |R|$ and $\tan \phi$. The standing wave pattern due to the reflection at a plane plasma and at a perfect metal are shown, respectively, by solid and dotted lines in Figure 25. The normalized signal amplitudes, h_1 and h_2, which are functions of the electric fields at these points, are related to $|R|$ and ϕ by means of the equations,

$$h_1 = \frac{1}{4} \left| 1 - |R| \; e^{j\phi} \right|^2 = \frac{1}{4} \left\{ (1 - |R| \cos \varphi)^2 + |R|^2 \sin^2 \phi \right\} \tag{19}$$

$$h_2 = \frac{1}{4} \left| 1 + |R| \; e^{j\phi} \right|^2 = \frac{1}{4} \left\{ (1 + |R| \cos \varphi)^2 + |R|^2 \sin^2 \phi \right\} \tag{20}$$

In deriving these it is assumed that the crystal is a square low detector. Figure 26 shows h_1 and h_2 for different values of ϕ and $|R|$. By solving Equations (19a) and (19b)

$$|R| = \frac{h_2 - h_1}{\cos \varphi} = \left\{ 2(h_1 + h_2) - 1 \right\}^{1/2} \tag{20a}$$

$$\sin \phi = \left\{ 1 - \frac{(h_2 - h_1)^2}{2(h_1 + h_2) - 1} \right\}^{1/2} \tag{20b}$$

The small changes ΔR and $\Delta \phi$ in $|R|$ and ϕ which cause the small deviations Δh_1 and Δh_2 in h_1 and h_2 are, from (20a) and (20b),

$$\Delta R = \frac{\Delta h_2 - \Delta h_1}{|R|} = \frac{\Delta h_1 + \Delta h_2 - |R| \sin \phi \, \Delta \phi}{\cos \phi} \tag{21a}$$

$$\Delta \phi = \frac{\Delta h_1 + \Delta h_2 - \cos \phi \, \Delta R}{R \sin \phi} \tag{21b}$$

If the gas is fully ionized, or nearly so, ν is a function of the electron temperature T_e and electron density n.

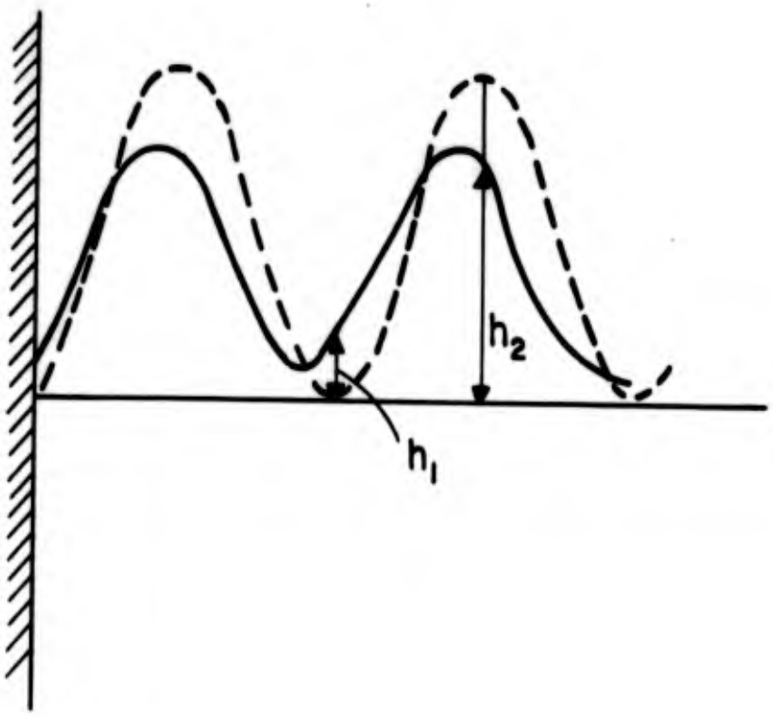

Figure 25. Standing wave patterns due to a high density plasma and a perfect conductor. (Solid line: for plasma, dashed line: for perfect conductor)

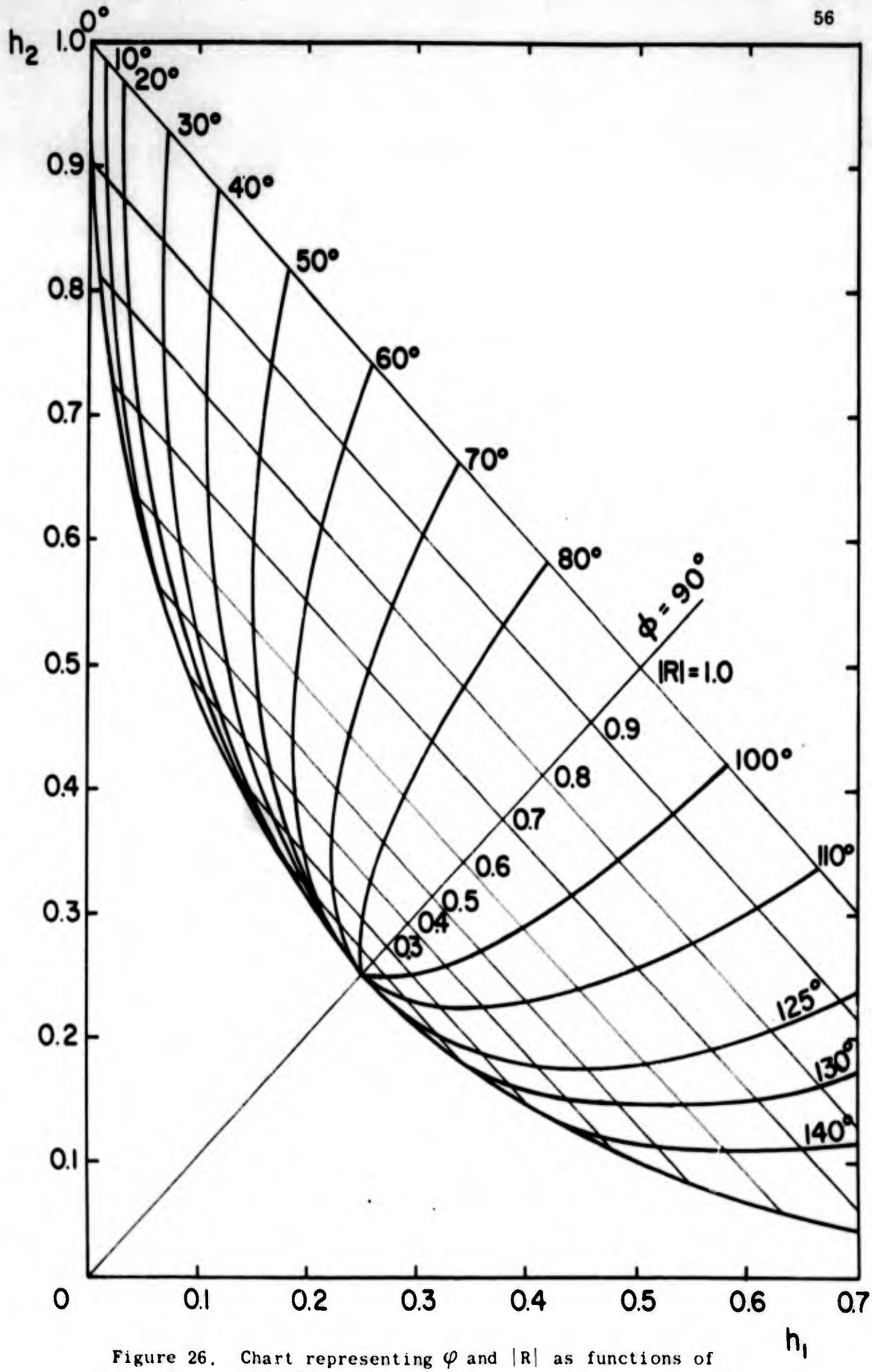

Figure 26. Chart representing φ and $|R|$ as functions of h_1 and h_2

$$\nu = 3.60\ n\ T_e^{-3/2} \log\left(1.25 \times 10^4\ \frac{T_e^{3/2}}{n^{1/2}} \right) \qquad (22)$$

This equation can be obtained from the collision characteristic time between ions and electrons. In Figures21 and 23 the dotted lines correspond to constant electron temperature for 9300 mc.

Thus, the electron density can be found from 1 - |R| or tan ϕ if the electron temperature is known. When $\omega_p^2/\omega^2 \gg 1$, the electron density, the collision frequency, and the electron temperature can be calculated from Equations (16a), (16b) and (22).

When the wave propagates in a waveguide, (14a) and (14b) should be modified as

$$\alpha^2 = \frac{k_o^2}{2}\left[\left\{1 - \left(\frac{\lambda}{\lambda_o}\right)^2 - \frac{\omega_p^2/\omega^2}{1 + (\nu/\omega)^2}\right\} + \left\{\left(1 - \left(\frac{\lambda}{\lambda_o}\right)^2 - \frac{\omega_p^2/\omega^2}{1 + (\nu/\omega)^2}\right)^2 + (\nu/\omega)^2\left(\frac{\omega_p^2/\omega^2}{1 + (\nu/\omega)^2}\right)^2\right\}^{1/2}\right] \qquad (14e)$$

$$\beta^2 = \frac{k_o^2}{2}\left[\left\{1 - \left(\frac{\lambda}{\lambda_o}\right)^2 - \frac{\omega_p^2/\omega^2}{1 + (\nu/\omega)^2}\right\} + \left\{\left(1 - \left(\frac{\lambda}{\lambda_o}\right)^2 - \frac{\omega_p^2/\omega^2}{1 + (\nu/\omega)^2}\right)^2 + (\nu/\omega)^2\left(\frac{\omega_p^2/\omega^2}{1 + (\nu/\omega)^2}\right)^2\right\}^{1/2}\right] \qquad (14f)$$

where λ_o is the cut-off wavelength of the waveguide. The reflection coefficient is also somewhat modified.

When a microwave propagates in a waveguide and passes through a glass wall before being reflected at the plasma surface, as shown in Figure 27, corrections are necessary.

Assuming that the dielectric constant and the thickness of the glass wall are ϵ and ℓ, respectively, then the total complex reflection coefficient

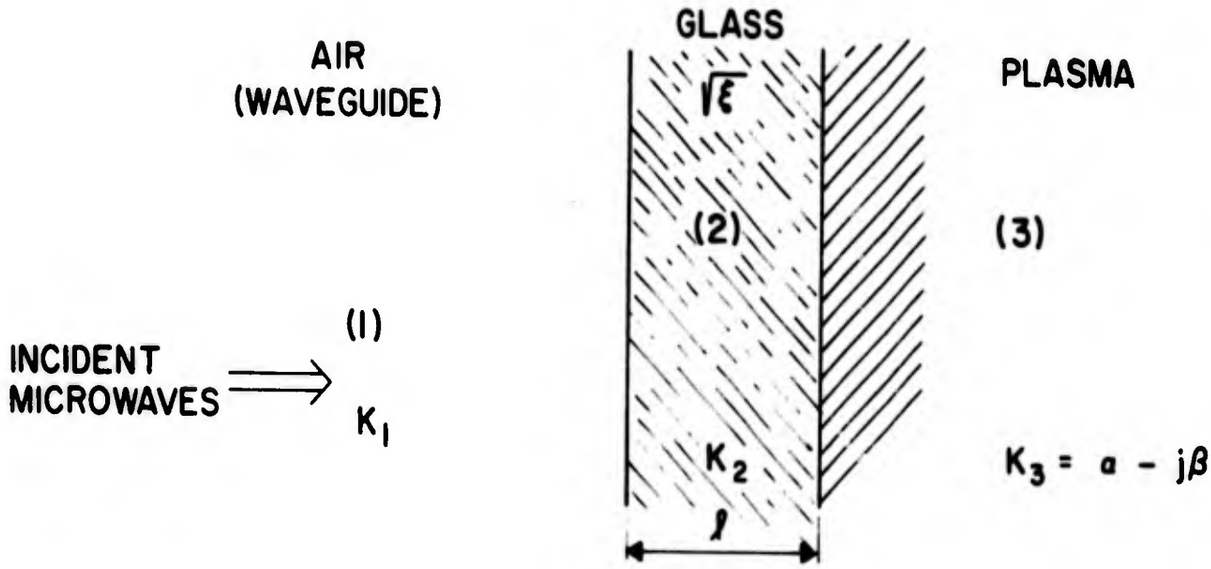

Figure 27. Schematic for the theoretical calculation of the complex reflection coefficient

is solved from four boundary conditions at two discontinuous surfaces. According to the arrangement shown in Figure 27;

$$|R|\, e^{j\theta} = \frac{1 - k_3/k_1 - j(k_2/k_1 - k_3/k_2)\tan k_2 \ell}{1 + k_3/k_1 + j(k_2/k_1 - k_3/k_2)\tan k_2 \ell} \tag{23}$$

where k_1, k_2 and k_3 are the propagation constants in free space, glass, and plasma, respectively, and ℓ is the thickness of the glass wall. Since $k_2/k_1 = \sqrt{\epsilon}$, $k_3/k_2 = k_3/k_1 \quad 1/\sqrt{\epsilon}$, it can be rewritten as,

$$|R|\, e^{j\theta} = \frac{k_1(1 - j\sqrt{\epsilon}\tan k_2 \ell) - k_3(1 - j\,{}^1/\sqrt{\epsilon}\tan k_2 \ell)}{k_1(1 + j\sqrt{\epsilon}\tan k_2 \ell) + k_3(1 - j\,{}^1/\sqrt{\epsilon}\tan k_2 \ell)}$$

$$= \frac{k_1(\chi - jY) - (\alpha - j\beta)}{k_1(\chi + jY) + (\alpha - j\beta)} \cdot \frac{1 - j\,{}^1/\sqrt{\epsilon}\tan k_2 \ell}{1 + j\,{}^1/\sqrt{\epsilon}\tan k_2 \ell} \tag{24}$$

where

$$\frac{1 \mp j\sqrt{\epsilon}\tan k_2 \ell}{1 \mp j\,{}^1/\sqrt{\epsilon}\tan k_2 \ell} = \frac{1 + \tan^2 k_2 \ell}{1 + {}^1/_{\epsilon}\tan^2 k_2 \ell} \mp j\,\frac{\tan k_2 1\ (\sqrt{\epsilon} - {}^1/\sqrt{\epsilon})}{1 + {}^1/\epsilon \tan^2 k_2 \ell}$$

$$\equiv \chi \mp j\,Y$$

$$k_3 \equiv \alpha - j\beta$$

The ratio of the imaginary to the real parts of the first term in Equation (24) is the phase angle $\tan\theta$ of the reflection coefficient

$$\tan\ \phi = -\tan\theta = \frac{-2k_1\,\chi\,(\beta - k_1 Y)}{k_1(\chi^2 - Y^2) - \alpha^2 - \beta^2 + 2k_1\,\beta\,Y}$$

which, for high electron density, can be expanded and is seen to be proportional to

$$\doteq \frac{2 k_1 \beta}{\alpha^2 + \beta^2} \left(\times \left(1 + \frac{2 k_1 \beta Y}{\alpha^2 + \beta^2} \right) \cdot \left(1 - \frac{k_1 Y}{\beta} \right) \right.$$

The second and third terms of this expression are the correction factors brought about by the glass boundaries. Similarly, the constant phase shift ϕ_o due to the presence of the glass can be obtained from the second term of Equation (24)

$$\tan \phi_o = - \tan \theta_o = \frac{2/\sqrt{\epsilon} \tan k_2 \ell}{1 + 1/\epsilon \tan^2 k_2 \ell} \qquad (25)$$

The total phase shift ϕ is the sum of ϕ_o and ϕ'. Therefore, the constant value of ϕ_o should be substracted from the measured ϕ. When k_1 is the propagation constant in the waveguide, it should be replaced by $k_o \sqrt{1 - (\lambda/\lambda_o)^2}$, where k_o is the free space propagation constant.

Finally,

$$\tan \phi = \frac{2 \beta k_o}{\alpha^2 + \beta^2} \left\{ 1 - (\lambda/\lambda_o)^2 \right\}^{1/2} \left\{ \frac{1 + \tan^2 k_2 \ell}{1 + 1/\epsilon \tan^2 k_2 \ell} \right\} \left\{ 1 + \frac{2 k_1 \beta Y}{\alpha^2 + \beta^2} \right\} \left\{ 1 - \frac{k_1 Y}{\beta} \right\} \qquad (26)$$

The two last parentheses in Equation (26) can be neglected only for large β or for high electron density. On the other hand, when ℓ is a multiple of a half wavelength or very small, all the correction terms due to the presence of the glass wall disappear.

10. EXPERIMENTAL PROCEDURES AND RESULTS

The discharge tube shown in Figure 28 is 30 mm in outside diameter, 1.3 mm in glass thickness, and about 25 cm in length. The two electrodes are connected at its extremities. A 2.5 μF, 7.5 kv condenser discharge is ignited between these two electrodes by firing a thyratron. Measurements are carried on with a flat waveguide (4 mm height and 33 mm width), connected to the standard waveguide system through a tapered section. The discharge tube passes through the waveguide so that the electric field is perpendicular to the tube axis.

The movable probe detectors are adjusted so that one is at the minimum and the other at the maximum amplitude of a perfect standing-wave pattern caused by a short at the end of the flat waveguide. This short acts as a reference in the measurements of the reflection coefficient. The maximum amplitude h_m of the detector signal, which is necessary to normalize the probe signal amplitudes h_1 and h_2, can be found from the magnitude of the cut-off pulse of the h_2 trace. Figure 29 shows typical simultaneous oscilloscope traces of h_1 and h_2 after the tube was ignited by a condenser discharge. The traces in (a) are expanded four times over that in (b) to show the small changes of h_1 and h_2 more accurately.

Even at the beginning of the afterglow ($t \cong 0$) where extremely high electron density may be assumed, h_1 is not zero and the high density plasma, which appears behind the glass wall, apparently does not make a perfect short circuit. The glass wall effect, as calculated previously, maintains a constant phase shift ϕ_o. Moreover, the value of $|R_0|$ is less than unity since a fraction of the incident wave energy is lost by scattering along the glass. The two parameters, ϕ_o and $|R_o|$, can be calculated from Equations (20a) and (20b) for the values of h_1 and h_2, measured at $t = 0$. Then the electron density n can be deduced from the time varying Δh_1 and Δh_2, by means of Equations (21a) and (21b), assuming small values of ν/ω. The electron density of 50 μsec and 75 μsec was calculated by this method. After t = 100 μsec, n was calculated again by Equations (20a) and (20b), where now the constant ϕ_o was subtracted from the measured ϕ.

As is seen in Figure 25, better sensitivity in h_1 and h_2 with respect to small changes of ϕ is expected at some fixed position ϕ_o' of the probes other than $\phi_o' = 0^o$ or $\phi_o' = 180^o$. Therefore, if a thin mica window is used instead of the

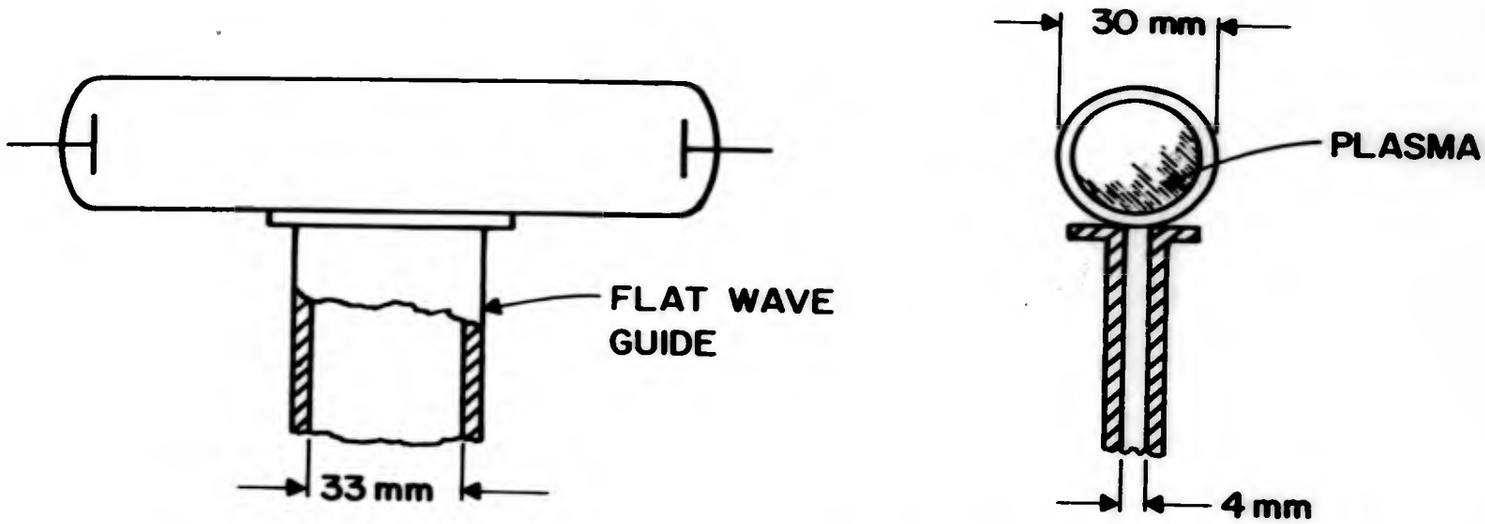

Figure 28. Arrangement of the discharge tube and the waveguide

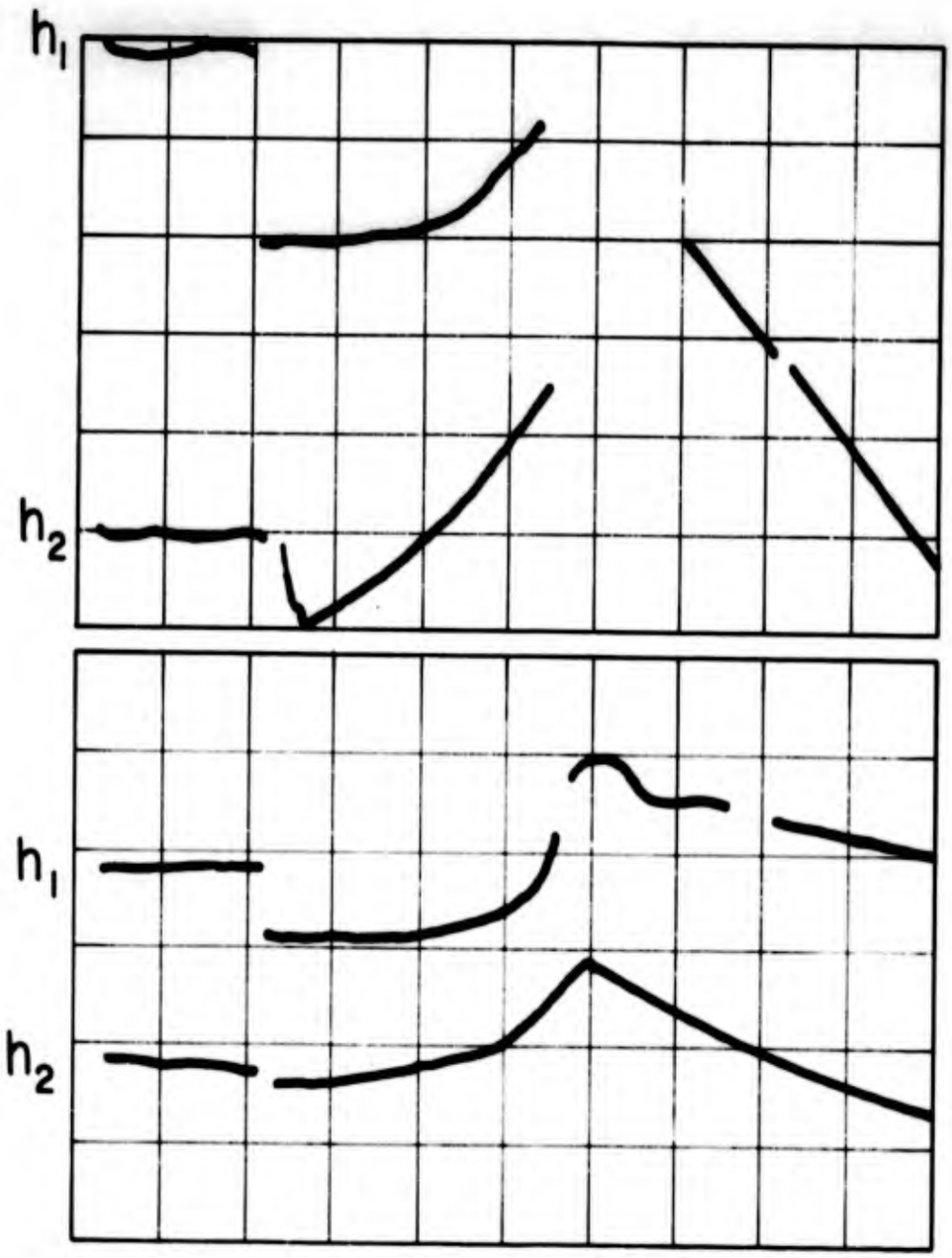

Figure 29. Simultaneous display of h_1 and h_2. Upper traces are expanded four times

glass wall in order to eliminate the correction described in section 9, the probe detectors should be shifted out of their initial minimum or maximum amplitude positions to new positions having larger slopes $\Delta h/\Delta \phi$. For instance, a normalized amplitude change $\Delta h_1 = 0.01$ (1 mm for $h_m = 100$ mm) yields a 1^o change in the electrical phase angle for $\phi_o' = 90^o$, if ΔR is neglected. This phase angle corresponds to $n = 10^{16}$ cm^{-3} at a frequency of 9000 mc.

Figure 30 shows the electron density decay curve, calculated from the recorded traces in Figure 29, where the gas is initially assumed to be perfectly ionized. Since in this calculation the apparent value of $|R|$ is not simply known, the effect of ν was neglected. The effects of the first two correction terms in Figure 26 are less than the experimental errors and are disregarded. The value of ψ_o in Equation (25) is $= 29^o$, which is close to the value of 30^o measured at $t = 0$.

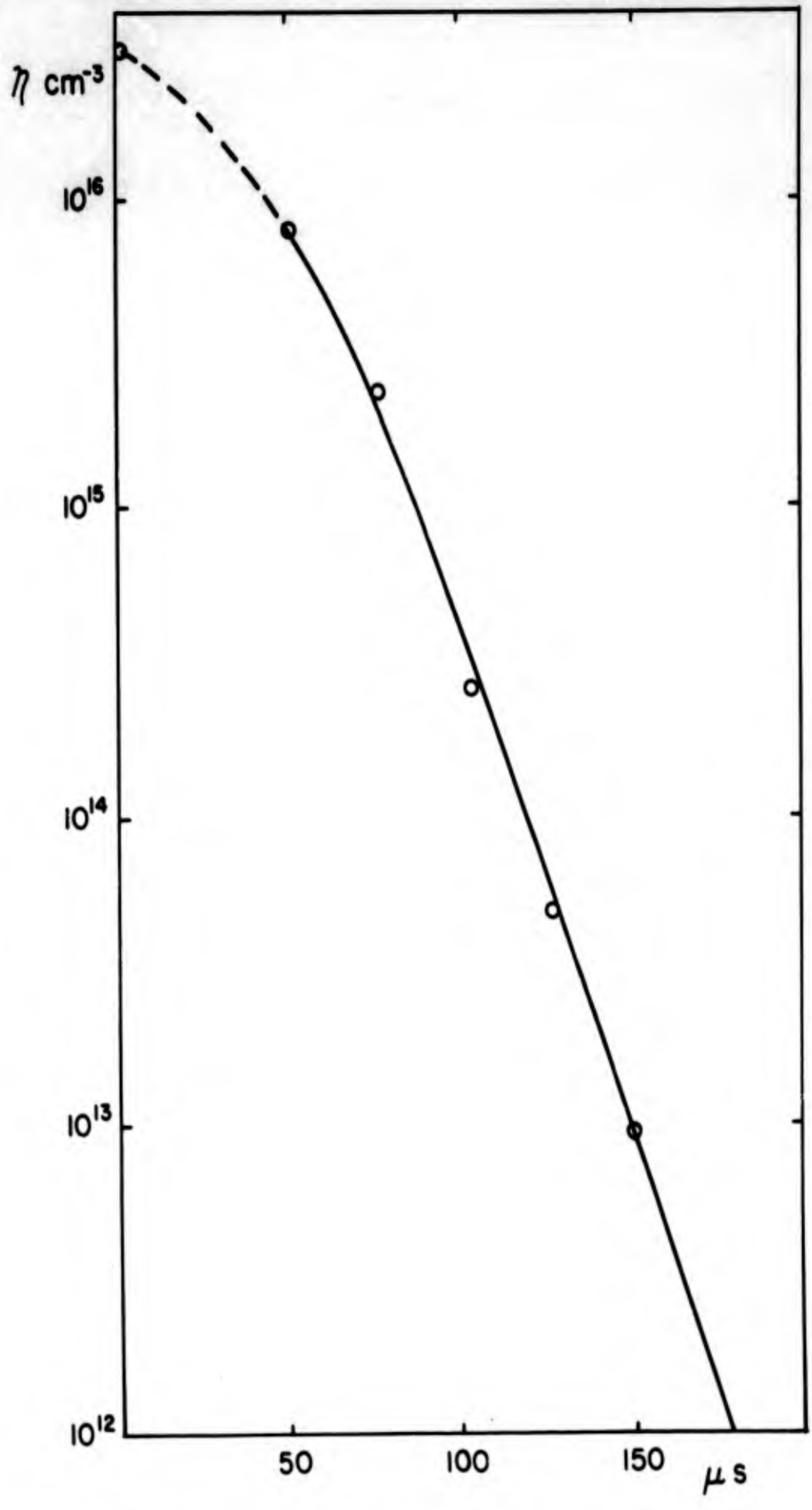

Figure 30. Electron decay curve calculated from Figure 29

REFERENCES

1. A. A. Dougal and L. Goldstein, IRE Transaction ED-3 142(1956)
2. R. L. Rayleigh , Proc. Roy. Soc. A 183 26(1944)
3. R. F. Fowler, Phys. Rev. 82 879(1951)
4. M. M. Cloupeau, C. R. 244 2033 (1957)
5. R. M. Roger der Agobian, C. R. 248 1308(1959)
6. D. L. Schultz, The fourth international Conference of Ionization Phenomena in Gases 2 1118(1959)
7. S. J. Buchsbaum and S. C. Brown, Phys. Rev. 106 196(1957)
8. V. Josephson, J. of Appl. Physics 29 30(1958)
9. A. Kantrowitz, J. of Appl. Physics 26 1392 Fig. 3(a) (1956)
10. E. H. Cullington, W. G. Chace and R. L. Morgan, Electronics 86(1958)
11. N. Markuvitz, Radiation Laboratories Series 10 266
12. V. L. Ginsburg, J. Phys. (USSR) 8 253(1944)
13. A. L. Gilardini and S. C. Brown, Phys. Rev. 100 1037 (1955)
14. A. Kantrowitz, J. of Appl. Physics 26 106 Fig 7 (1955)
15. L. Spitzer, "Physics of Fully Ionized Gases" 80 Eq. (5-31)
16. A. A. Dougal and L. Goldstein, Phys. Rev. 109 615(1958)
17. J. M. Anderson and L. Goldstein, Phys. Rev. 100 1037 (1955)
18. A. Kantrowitz, J. of Appl. Physics 23 1390 (1952)
19. L. Spitzer, "Physics of Fully Ionized Gases" 50 Eq. (4-4)

Contract DA 36-039-SC-78313

DISTRIBUTION LIST

OASD (R&E), Rm. 3E1065
Attention: Technical Library
The Pentagon
Washington 25, D. C.

Chief of Research and Development
Dept. of the Army
Washington 25, D. C.

Director
Attention: Code 2027
U. S. Naval Research Laboratory
Washington 25, D. C.

Commanding Officer and Director
U. S. Navy Electronics Laboratory
San Diego 52, California

*Commander
Attention: ASAPRL
Aeronautical Systems Div.
Wright-Patterson Air Force Base
Ohio (2 copies)

Commander, AF Com. & Control Dev. Div.
Air Research and Development Command
United States Air Force
L. G. Hanscom Field
Bedford, Massachusetts

Attention: CROTL
CCRR
CCSD
CRZC

Commander
Attention: RAALD
Rome Air Development Center
Griffiss Air Force Base, New York

Chief Signal Officer
Attention: SIGRD-4a
Department of the Army
Washington 25, D. C.

Commanding Officer
Attention: SIGRA/SL-PRM (records file copy)
U. S. Army Signal Res. & Dev. Lab.
Fort Monmouth, New Jersey

Commander
Attention: TIPCR
Armed Services Tech. Info. Agency
Arlington 12, Virginia (10 copies)

Commanding Officer
Attention: Library, Rm. 211, Bldg. 92
Diamond Ordnance Fuze Labs.
Washington 25, D. C.

Commanding Officer
U. S. Army Signal Electronics Res. Unit
P. O. Box 205
Mountain View, California

Chief, U. S. Army Security Agency
Arlington Hall Station
Arlington 12, Virginia (2 copies)

Commanding Officer
U. S. Army Signal Material Support Agency
Attention: SIGMS-ADJ
Fort Monmouth, New Jersey

Corps of Engineers Liaison Office
U. S. Army Signal Res. & Dev. Lab.
Fort Monmouth, New Jersey

Commanding Officer
Attention: Technical Documents Center
U. S. Army Signal Res. & Dev. Lab.
Fort Monmouth, New Jersey

Commanding Officer
U. S. Army Signal Res. & Dev. Lab.
Fort Monmouth, New Jersey
Attention: Logistics Division
(For SIGRA/SL-PRM)(Project Engineer)

3 (already forwarded for approval)

Commander, Air Force Cambridge Res. Lab.
Attention: CRO
L. G. Hanscom Field
Bedford, Massachusetts

AFSC Liaison Office
Naval Air R & D Activities Command
Johnsville, Pennsylvania

Contract DA 36-039-SC-78313

DISTRIBUTION LIST (Continued)

Commanding Officer
Attn: Technical Information Division
(FOR RETRANSMITTAL TO ACCREDITED BRITISH AND CANADIAN GOVERNMENT REPRESENTATIVES) & Ministry of Supply, Royal Radar Establishment
St. Andrew's Road, Malvern,
Worcestershire, England,
Attn: Alan F. Gibson
U. S. Army Signal Res. & Dev. Lab.
Fort Monmouth, New Jersey (3 copies)

Commanding Officer
Attention: ORDBA-FEL
Frankford Arsenal
Philadelphia 37, Pennsylvania

Autonetics
A Division of North American Aviation Inc.
9150 E. Imperial Highway
Attention: Technical Library
Dept/3041-13-5877
Bldg. 2
Downey, California

Deputy President
U. S. Army Security Agency Board
Arlington Hall Station
Arlington 12, Virginia

Bomac Laboratories
Attention: Dr. A. O. McCoubrey
Beverly, Massachusetts

The University of Michigan
3505 E. Engineering Bldg.
Ann Arbor, Michigan

Commanding Officer
Attention: Director of Research
U. S. Army Signal Res. & Dev. Lab.
Fort Monmouth, New Jersey

Commanding General
Attention: Technical Library
Redstone Arsenal
Huntsville, Alabama

Chief, Bureau of Ships
Attention: 691A1
Department of the Navy
Washington 25, D. C.

Chief of Ordnance
Attention: ORDTX-AR
Washington 25, D. C.

Marine Corps Liaison Office
U. S. Army Signal Res. & Dev. Lab.
Attention: SIGRA/SL-LNR
Fort Monmouth, New Jersey

Advisory Group on Electron Devices
346 Broadway
New York 13, New York (2 copies)

DISTRIBUTION LIST (Continued)

Dr. Roger P. Wellinger
Supervisor, Gas Gas Discharge Dev. Unit
I and T Tube Sub-Department
General Electric Company
Schenectady 5, New York

Dr. W. H. Christoffers
Hughes Research and Development Lab.
Microwave Tube Department
Culver City, California

Dr. Richard Slattery
MIT Lincoln Laboratory
Lexington 73, Massachusetts

Dr. Howard Holt
Rensselaer Polytechnical Institute
Electrical Engineering Dept.
Troy, New York

Mr. Nathan R. Einhorn
Assistant Chief
Exchange and Gift Division
The Library of Congress
Washington 25, D. C. (2 copies)

Dr. Meyer Gilden
Research Engineer
Electromagnetics Lab.
Stanford Research Institute
Menlo Park, California

Dr. T. N. Morgan
IBM Corporation
Research Center
Yorktown, New York Hights

Dr. Amikam Aharoni
Weizmann Institute of Science
Rehovoth, Israel

Dr. Karl H. Seeger
Zweites Physikalisches Institut
der Universitat Heidelberg
Philosophenweg 12
Heidelberg, Germany

Dr. Kenneth Rose
General Electric Research Laboratory
Schenectady, New York

Dr. Harry Letaw, Jr.
Martin Company
Electronics Division
Baltimore, Maryland

Dr. R. C. Gunton
Lockheed Missile & Space Company
Department 53-22, Bldg. 202
Palo Alto, California